A unified general framework for small and finite strain two-invariants elastoplasticity

Abstract

Purpose - This paper proposes a unified original general framework, designed to theoretically develop and to extremely easily implement elastoplastic constitutive laws defined in the so called *two-invariants space*, both in small and finite strain regime.

Design/methodology/approach - A general return mapping algorithm is proposed, and particularly a standard procedure is developed to compute the two algorithmic tangent operators, required to solve the Newton-Raphson scheme at the local and global level, and thus cast the elastoplastic algorithm within a FEM code.

Findings - This work demonstrates that the proposed procedure is fully general, and can be applied whatever is the elastic law, the yield surface, the plastic potential function and the hardening law. Several numerical examples are reported, not only to demonstrate the accuracy and robustness of the algorithm, but also explain how to use this general algorithm also in other applications.

Originality/value - The proposed algorithm and its numerical implementation into a FEM code is new and original. The usefulness and the value of the algorithm is twofold: (i) it can be implemented in a small and finite strain simulation FEM code, in order to handle different types of constitutive laws in the same modular way, thus fully leveraging on modern object-oriented coding approach; (ii) it can be used as a framework to develop (and then to implement) new constitutive models, since the researcher can simply define the relevant functions (and its first and second derivatives), and easily get the numerical algorithm.

Preprint submitted to Engineering Computations *April 6, 2022*

Keywords: FEM, return mapping algorithm, elastoplasticity, finite strain

1. Introduction

The mechanical behavior of many materials, such as soil, rock, concrete, metal, ceramic and plastic, is characterized by an elastoplastic response, which is crucial to be captured for a correct and reliable design of structures and manufactured goods. The description of the elastoplastic material behaviour is a challenging task, from both an experimental and a numerical point of view, since specific algorithms are required in order to implement elastoplastic constitutive laws into a FEM simulation code. Moreover, the implementation is particularly arduous when assuming a finite strain regime, since non-linear material together with non-linear geometry effects must be taken into account.

To define an elastoplastic model, many aspects need to be addressed by means of proper functions, namely: the elastic law, the yield function(s), the plastic potential function(s) and the hardening law(s). Depending on their choice, a large amount of elastoplastic models has been proposed (the reader should refer to classical works such as Khan & Huang (1995), Aubertin & Li (2004), Simo & Hughes (2006), de Souza Neto et al. (2009), Bao et al. (2013) and Borja (2013)). Among all the numerous available constitutive laws, some of them share a common feature, i.e. the fact that the aforementioned functions, which identify the constitutive model, are defined in a so called *two-invariants space*. In other words, all the functions depend on the two-invariants, determined in terms of strain measures via the volumetric and deviatoric strain

$$\epsilon_v^e = \boldsymbol{\epsilon}^e \cdot \boldsymbol{\delta}; \qquad \epsilon_s^e = \sqrt{\frac{2}{3}}\,\|\boldsymbol{e}^e\|\,; \qquad \boldsymbol{e}^e = \boldsymbol{\epsilon}^e - \frac{1}{3}\epsilon_v^e\boldsymbol{\delta}, \tag{1}$$

with $\boldsymbol{\epsilon}^e = (\epsilon_1^e, \epsilon_2^e, \epsilon_3^e)^T$ the vector of the principal components of the elastic strain tensor $\boldsymbol{\epsilon}$, $\boldsymbol{\delta} = (1,1,1)^T$ and $\|\cdot\|$ denotes the euclidean norm (see the end of this section for the notation convention). In terms of stress measures, the

Identification	Yield function $\mathscr{F}$
von Mises	$\mathscr{F} = Q - c$
Mises-Schleicher	$\mathscr{F} = Q - \sqrt{3(\sigma_c - \sigma_t)P + \sigma_c\sigma_t}$
Drucker-Prager	$\mathscr{F} = Q - mP - c$
Modified Cam-Clay	$\mathscr{F} = (Q/M)^2 + P(P - P_c)$
Cap Model	$\mathscr{F}_1 = Q + \gamma\exp(-\beta P) - \alpha$
	$\mathscr{F}_2 = (\frac{RQ}{\sqrt{3}})^2 + (3P - C)^2 - R^2b^2$
Shima-Oyane	$\mathscr{F} = (Q/\sigma_M)^2 + a_1n^{a2}(P/\sigma_M)^2 - (1-n)^5$
Gurson	$\mathscr{F} = (Q/\sigma_M)^2 + 2n\cosh(\frac{3}{2}\frac{P}{\sigma_M}) - (1+n^2)$
Modified Gurson	$\mathscr{F} = (Q/\sigma_M)^2 + 2q_1n\cosh(\frac{3}{2}\frac{q_2P}{\sigma_M}) - (1+(q_1n)^2)$
Lee and Oung	$\mathscr{F} = Q^2 + \frac{9}{4}nP^2 + 3(1-n)(T-C)P - (1-n)^2CT$

Table 1: Most common elastoplastic laws for engineering materials defined in the two-invariants space (after Aubertin & Li (2004)). (Note: for the interested reader, the meaning of each single parameter can be found in the above mentioned reference. The yield function may be defined in a $[P, Q]$ space or equivalently in a $[I_1(= 3P), \sqrt{J_2}(= Q/\sqrt{3})]$ space.)

two-invariants are expressed via the mean normal stress P and the deviatoric stress Q

$$P = \frac{1}{3}\boldsymbol{\varsigma}\cdot\boldsymbol{\delta}; \qquad Q = \sqrt{\frac{3}{2}}\,\|\boldsymbol{s}\|\,; \qquad \boldsymbol{s} = \boldsymbol{\varsigma} - P\boldsymbol{\delta}, \tag{2}$$

with $\boldsymbol{\varsigma} = (\sigma_1, \sigma_2, \sigma_3)^T$ the vector of the principal components of the stress tensor $\boldsymbol{\sigma}$.

Some of the most known and used elastoplastic laws for engineering materials defined in the two-invariants space are summarized in Table 1 (Aubertin & Li, 2004). The list does not pretend to be exhaustive, and only the yield function is reported, but still it is useful to recall the most relevant ones.

More recently, many other elastoplastic constitutive laws based on invariants have been proposed and frequently adopted in various applications. For instance, Weng & Ling (2013) proposed a constitutive model for the behavior of sandstone, based on the generalized plasticity concept, defined in the two-invariants space. Lai et al. (2016) investigated the mechanical behavior of frozen saline sandy soil, with a yield function in the (P, Q) domain considering the influence of salt contents. Spiezia et al. (2016) proposed a two-invariants elastoplastic model for highly porous rocks. Carvalho et al. (2018) investigated the yielding behaviour of ductile porous materials through computational homogenization. Coelho & Roehl (2019) proposed a finite–strain elastoplasticity material model for ETFE membrane structures. Indriyantho et al. (2020) investigated the non-local softening plasticity for concrete at finite strains. Rawat et al. (2021) proposed a nonlocal plasticity-based damage model using an isogeometric approach for quasi-brittle materials. In the formulation of a new constitutive law, usually based on the experimentally observed material behaviour, one of the most critical task is its implementation into a FEM code. Especially in non linear laws, the correct implementation of the tangent operators is fundamental to achieve quadratic convergence, and hence to obtain a fast and robust implementation. This paper presents an original unified general algorithm to numerically solve elastoplastic constitutive models based on two-invariants. The idea consists in writing a general return mapping algorithm, such that the consistent tangent operators are computed autonomously by the framework. The framework implements a standard procedure to compute Jacobi matrix of the return mapping equations (used by the material subroutine in the *local* Newton iteration at the Gauss point level) and consistent tangent operator in the principal space (used by the finite element program to construct the overall tangent operator for *global* Newton iteration), whatever is the elastic law, the yield surface, the plastic potential function and the hardening law.

There are two main reasons why this framework is useful:

1. *Modular implementation*: the algorithm can be implemented in both a small and finite strain FEM code, in order to handle different type of constitutive laws in the same modular way, hence avoiding to repeat pieces

of code that perform the same tasks. This approach is important to fully leverage on modern object-oriented FEM codes Yilmaz (2019);

2. *New model development*: the algorithm can be used to implement and develop new constitutive models, since the researcher can simply focus on the governing functions (with its first and second derivatives), and easily obtain the numerical algorithm, which is usually a tedious and tough task to fulfil. In particular, the proposed algorithm provides the tangent operators for the non linear iterative schemes.

Moreover, the algorithm combines several positive features: (i) it can be used whatever is the elastic law, the yield surface, the plastic potential function and the hardening law, (ii) it handles small and finite strain constitutive laws, (iii) it is based on a fully implicit unconditionally stable implementation, (iv) it relies on hyperelasticity which is, unlike hypoelasticity, thermodynamically consistent, (v) it guarantees quadratic convergence both at local (stress integration) and global (equilibrium equation) level, if implemented in non-linear FE codes.

This formulation is original and has never been proposed before. A similar approach was proposed by Aravas (1987) and Govindarajan & Aravas (1995) for general pressure-dependent plasticity models, even though the way in which finite strain is taken into account is different. Additionally, the elastic part is now not necessarily linear, but it can be defined via a fully general free energy function. Moreover, this paper provides directly the partial derivatives matrices, and therefore implementing the algorithm in a FE code is much easier and straightforward.

Also in recent years, there has been a keen interest to define unified frameworks that can incorporate different approaches into a single - more general - one, as testified by several works, such as Peng & Chen (2012); Cecilio et al. (2015); Hu et al. (2017); Gudimetla & Doghri (2017); Halilovic et al. (2017); Mourad et al. (2017); Tavoosi et al. (2019); Čermák et al. (2019); Neuner et al. (2020).

The paper is organized as follows: Section 2 briefly recalls the theoretical framework for the solution of an elastoplastic boundary-value problem, considering small and finite deformations. Section 3 introduces the two-invariants space for the solution of the return mapping algorithm, underlining the key aspects of the formulation. Section 4 presents the unified general algorithm to solve the return mapping algorithm in the two-invariants space. Several numerical results are presented in section 5, showing how two common constitutive models can be treated by the proposed algorithm, together with the advantages of the proposed formulation. In particular, the developed framework has been applied to two very well known constitutive laws, namely the Drucker-Prager and the Modified Cam Clay. The choice of these two popular constitutive laws was motivated by the fact that the reader can easily understand how the framework works, and therefore apply and extend it to new models. Nevertheless, these two models are still involved in recent research activity (see e.g. Isbuga & Regueiro (2017); Zhao et al. (2019); Mohammadi et al. (2019); Späth et al. (2021); Lee et al. (2021) for the DP models and De la Morena et al. (2017); Lloret-Cabot et al. (2018); Wei et al. (2021); Sanei et al. (2020) for the MCC model).

The following rules apply for notations: bold-face letters denote matrices and vectors; the symbol '$\cdot$' denotes an inner product of two vectors (e.g. $\boldsymbol{a}\cdot\boldsymbol{b} = a_i b_i$), or a single contraction of adjacent indices of two tensors (e.g. $\boldsymbol{c}\cdot\boldsymbol{d} = c_{ij}d_{jk}$); the symbol ':' denotes an inner product of two second-order tensors (e.g. $\boldsymbol{c} : \boldsymbol{d} = c_{ij}d_{ij}$), or a double contraction of adjacent indices of tensor of rank two and higher (e.g. $\boldsymbol{C} : \boldsymbol{\epsilon}^e = C_{ijkl}\epsilon^e_{kl}$); the symbol '$\otimes$' denotes a juxtaposition, e.g. $(\boldsymbol{a}\otimes\boldsymbol{b})_{ij} = a_i b_j$. For any symmetric second-order tensor $\boldsymbol{\alpha}$ and $\boldsymbol{\beta}$ we have $(\boldsymbol{\alpha}\otimes\boldsymbol{\beta})_{ijkl} = \alpha_{ij}\beta_{kl}$; $(\boldsymbol{\alpha}\oplus\boldsymbol{\beta})_{ijkl} = \alpha_{ik}\beta_{jl}$; and $(\boldsymbol{\alpha}\ominus\boldsymbol{\beta})_{ijkl} = \alpha_{il}\beta_{jk}$. Throughout the text, repeated indices are implicitly summed over, according to Einstein's convention, and positive stress is assumed for traction states, according to the solid mechanics convention.

2. Basic theoretical framework

This part of the work briefly recalls the theoretical background which allows to numerically solve an elastoplastic boundary-value problem. Both the small and finite strain formulation are recalled, highlighting how the two formulations lead to the same return mapping algorithm. Only the essential aspects are presented, but the reader should refer to de Souza Neto et al. (2009) and Borja (2013) for further details.

2.1. Small strain formulation

Let us consider the variational form of the linear momentum balance equation which, for quasi-static loading, reads

$$\mathscr{W} = \int_{\Omega} (grad\boldsymbol{\eta} : \boldsymbol{\sigma} - \rho\boldsymbol{\eta} \cdot \boldsymbol{g}) dV - \int_{\partial\Omega} \boldsymbol{\eta} \cdot \boldsymbol{t} dA = 0 \tag{3}$$

where ρ is the mass density, $\boldsymbol{g}$ is the vector of gravity accelerations, $\boldsymbol{t}$ is the traction vector, $\boldsymbol{\eta}$ is the weighting function, Ω is the domain of integration, $\partial\Omega$ is the domain boundary and *grad* is the gradient operator. For dead loading, the linearization of this function with respect to the state $\mathscr{W}^0$ reads

$$L\mathscr{W} = \mathscr{W}^0 + \int_{\Omega} grad\boldsymbol{\eta} : \mathscr{C} : grad\delta\boldsymbol{u} - \int_{\partial\Omega} \boldsymbol{\eta} \cdot \delta\boldsymbol{t} dA = 0, \tag{4}$$

where $\boldsymbol{u}$ is the displacement field and $\mathscr{C}$ is the fourth-order tangent operator consistent with the linearization of $\boldsymbol{\sigma}$. The task of solving the linear momentum balance equation resides in finding the displacement field $\boldsymbol{u}$, such that the stress $\boldsymbol{\sigma}$ satisfies the Eq. (3). In the context of elastoplasticity, Eq. (3) is solved incrementally, by means of *fictitious* time steps $[t_n, t_{n+1}]$, not related to any dynamic or transient phenomenon. The subscripts n denotes given initial values at the converged time step, while the subscripts $n+1$, which will be omitted for the sake of simplicity, denotes the unknown values at the current time step. The value of the stress at time step $n+1$ is given solving the return mapping equation

$$\boldsymbol{\sigma} = \boldsymbol{\sigma}^{Tr} - \Delta\lambda \mathscr{C}^e : \frac{\partial \check{\mathscr{G}}}{\partial \boldsymbol{\sigma}} \tag{5}$$

where $\boldsymbol{\sigma}^{Tr}$ is the *Trial* elastic stress predictor, $\Delta\lambda$ is the discrete plastic multiplier, $\mathscr{C}^e$ is the fourth order elastic tensor and $\check{\mathscr{G}}(\boldsymbol{\sigma}, \bar{\boldsymbol{\xi}})$ is the plastic potential function, which depends on the current stress state $\boldsymbol{\sigma}$ and the current plastic internal variables $\bar{\boldsymbol{\xi}}$. Eq. (5) must be completed by the yield condition $\check{\mathscr{F}}$

$$\check{\mathscr{F}} = \check{\mathscr{F}}(\boldsymbol{\sigma}, \boldsymbol{\xi}) = 0 \tag{6}$$

along with the evolution of the plastic internal variables $\boldsymbol{\xi} = \boldsymbol{\xi}_n + \Delta\boldsymbol{\xi}$ and $\bar{\boldsymbol{\xi}} = \bar{\boldsymbol{\xi}}_n + \Delta\bar{\boldsymbol{\xi}}$. The procedure to obtain tensor $\boldsymbol{\sigma}$ at the current time step by solving simultaneously Eq. (5) and Eq. (6), written so far in the general space of stress, may be simplified considering the spectral representation (see Ogden (1997); Borja et al. (2003) for details and relevance of the spectral decomposition). In fact, assuming isotropy in the elastic response, the stress and strain tensor may be written as

$$\boldsymbol{\sigma} = \sum_{A=1}^{3} \sigma_A \boldsymbol{m}^{(A)}, \qquad \boldsymbol{\epsilon}^e = \sum_{A=1}^{3} \epsilon^e_A \boldsymbol{m}^{(A)}, \qquad \boldsymbol{m}^{(A)} = \boldsymbol{n}^{(A)} \otimes \boldsymbol{n}^{(A)} \tag{7}$$

where σ_A, ϵ^e_A and $\boldsymbol{n}^{(A)}$ are respectively the principal Cauchy stress, the principal elastic strain and principal directions, which are coincident.

Taking advantage of the spectral representation and the assumption of both plastic and elastic isotropy, Eq. (5) may be formulated in the principal strain space. Under this assumption, the principal directions of the stress, the elastic strain and the plastic flow coincide, and further they coincide with the principal directions of their trial values. Hence, Eq. (5) reads:

$$\epsilon^e_A = \epsilon^{e,Tr}_A - \Delta\lambda \frac{\partial \hat{\mathscr{G}}}{\partial \sigma_A}, \tag{8}$$

with $A = 1, 2, 3$; assuming isotropy of the yield surface, Eq. (6) may be reformulated in the principal space as

$$\hat{\mathscr{F}} = \hat{\mathscr{F}}(\sigma_A, \boldsymbol{\xi}) = 0. \tag{9}$$

The equation for computing σ^{Tr}_A may be derived by the definition of a proper free energy function, and reads $\sigma_A = \partial\hat{\Psi}(\epsilon^e_A)/\partial\epsilon^e_A$. Briefly, in order to compute the updated stress tensor $\boldsymbol{\sigma}$ the crucial task is the solution of the non-linear system given by Eq. (8) and Eq. (9)

$$\boldsymbol{r}(\boldsymbol{x}) = \begin{Bmatrix} \epsilon^e_A - \epsilon^{e\ Tr}_A + \Delta\lambda \frac{\partial \hat{\mathscr{G}}}{\partial \sigma_A} \\ \hat{\mathscr{F}}(\sigma_A, \boldsymbol{\xi}) \end{Bmatrix} = \boldsymbol{0}; \qquad \boldsymbol{x} = \begin{Bmatrix} \epsilon^e_A \\ \Delta\lambda \end{Bmatrix}; \qquad A = 1, 2, 3. \tag{10}$$

Following the proposed return mapping algorithm and taking advantage of the spectral decomposition, the tangent operator - crucial to guarantee the asymptotic quadratic convergence rate - may be constructed from eigenvectors as (Ogden, 1997):

$$\begin{aligned}\mathscr{C} = \frac{\partial \boldsymbol{\sigma}_{n+1}}{\partial \boldsymbol{\epsilon}_{n+1}} &= \sum_{A=1}^{3}\sum_{B=1}^{3} a_{AB}\boldsymbol{m}^{(A)} \otimes \boldsymbol{m}^{(B)} \\ &+ \frac{1}{2}\sum_{A=1}^{3}\sum_{B\neq A}^{3}\left(\frac{\sigma_B - \sigma_A}{\epsilon_B^{eTr} - \epsilon_A^{eTr}}\right)\left(\boldsymbol{m}^{(AB)} \otimes \boldsymbol{m}^{(AB)} + \boldsymbol{m}^{(AB)} \otimes \boldsymbol{m}^{(BA)}\right). \qquad (11)\end{aligned}$$

where $a_{AB} = \partial\sigma_A/\partial\epsilon_B^{eTr}$. Note that the second term in Eq. (11) may become indeterminate in case of repeated eigenvalues of the strain tensor. In this case, the expression $(\sigma_B - \sigma_A)/(\epsilon_B^{eTr} - \epsilon_A^{eTr})$ may be slightly perturbed or may by replaced by the expression $\partial(\sigma_A - \sigma_B)/\partial\epsilon_B^{eTr}$ (Ogden, 1997). To the authors' experience, the second choice is preferable.

In conclusion, the two crucial tasks to solve the elastoplastic BVP are: (i) the solution of the non-linear system in Eq. (10), and (ii) the computation of the tangent operator $a_{AB} = \partial\sigma_A/\partial\epsilon_B^{eTr}$ in Eq. (11), both operations performed in the space of principal directions. The complete procedure to compute the update state of the stress $\boldsymbol{\sigma}$ and the consistent tangent operator $\mathscr{C}$ is summarized in Table 2.

2.2. Finite strain formulation

Assuming finite strain, the variation form of the linear momentum balance, written with respect to the reference configuration, reads

$$\mathscr{W} = \int_{\Omega_0} (GRAD\boldsymbol{\eta} : \boldsymbol{P} - \rho_0\boldsymbol{\eta}\cdot\boldsymbol{G})dV - \int_{\partial\Omega_0} \boldsymbol{\eta}\cdot\boldsymbol{t}_0 dA = 0 \qquad (12)$$

where $\boldsymbol{P}$ is the unsymmetric first Piola-Kirchhoff stress tensor, ρ_0 is the mass density in the reference configuration, $\boldsymbol{G}$ is the vector of gravity acceleration, $\boldsymbol{t}_0$ is the nominal traction vector, Ω_0 and $\partial\Omega_0$ are, respectively, the problem domain and boundary in the reference configuration. The gradient operator $GRAD$ is a spatial differentiation with respect to the coordinates of the reference

Implicit elastic predictor/return mapping algorithm for small strain
1. Compute elastic deformation predictor: $\boldsymbol{\epsilon}^{e\,Tr} = \boldsymbol{\epsilon}^e_n + \Delta\boldsymbol{\epsilon}$
2. Perform spectral decomposition: $\boldsymbol{\epsilon}^{e\,Tr} = \epsilon_A^{e\,Tr}\boldsymbol{n}^{Tr\,(A)} \otimes \boldsymbol{n}^{Tr\,(A)}$.
3. Compute elastic stress predictor: $\sigma_A^{Tr} = \partial\hat{\Psi}(\epsilon_A^{e\,Tr})/\partial\epsilon_A^{e\,Tr}$
4. Check if yielding: $\hat{\mathscr{F}}(\sigma_A^{Tr}, \boldsymbol{\xi}_n) \geq 0$?
No: elastic step. Set $\epsilon_A^e \equiv \epsilon_A^{e\,Tr}$, $\sigma_A \equiv \sigma_A^{Tr}$, $\boldsymbol{\xi} \equiv \boldsymbol{\xi}_n$, $\bar{\boldsymbol{\xi}} \equiv \bar{\boldsymbol{\xi}}_n$
Yes: plastic step. Solve Eq. (10) and compute ϵ_A^e, σ_A, $\boldsymbol{\xi}$, $\bar{\boldsymbol{\xi}}$.
5. Get elastic strain $\boldsymbol{\epsilon}^e$ and stress $\boldsymbol{\sigma}$ tensors from ϵ_A^e and σ_A.
6. Compute consistent tangent operator a_{AB} and $\mathscr{C}$ with Eq. (11).
7. Store elastic strain tensor $\boldsymbol{\epsilon}^e$.

Table 2: Numerical procedure to compute the updated stress state and the consistent tangent operator at the element level for small strain elastoplasticity.

configuration. The stress tensor $\boldsymbol{P}$ is related to the symmetric Kirchhoff stress tensor $\boldsymbol{\tau}$ through the deformation gradient $\boldsymbol{F} = \partial\boldsymbol{\phi}/\partial\boldsymbol{X}$ via the relation $\boldsymbol{\tau} = \boldsymbol{P} \cdot \boldsymbol{F}^T$, and thus $GRAD\boldsymbol{\eta} : \boldsymbol{P} \equiv grad\boldsymbol{\eta} : \boldsymbol{\tau}$. Assuming dead loading, the linearization of Eq. (12) with respect to the state $\mathscr{W}^0$ reads

$$L\mathscr{W} = \mathscr{W}^0 + \int_{\Omega_0} grad\boldsymbol{\eta} : \mathscr{A} : grad\delta\boldsymbol{u}dV - \int_{\partial\Omega_0} \boldsymbol{\eta} \cdot \delta\boldsymbol{t}_0 dA, \tag{13}$$

where

$$\mathscr{A} = \boldsymbol{\alpha} - \boldsymbol{\tau} \ominus \boldsymbol{1}, \tag{14}$$

with $(\boldsymbol{\tau} \ominus \boldsymbol{1})_{ijkl} = \tau_{il}\delta_{jk}$. Elastoplasticity is treated in the framework of the multiplicative plasticity (Lee, 1969; Simo, 1992; Borja et al., 2003). The corner stone of the finite strain multiplicative plasticity is the multiplicative decomposition of the deformation gradient

$$\boldsymbol{F} = \boldsymbol{F}^e \cdot \boldsymbol{F}^p, \tag{15}$$

where $\boldsymbol{F}^e$ and $\boldsymbol{F}^p$ are, respectively, the elastic and plastic part of the deformation gradient.

From the reduced dissipation inequality (Borja (2013)), the expression of the

the plastic flow direction can be identified:

$$-\frac{1}{2}\mathscr{L}_v \boldsymbol{b}^e = \dot{\lambda}\frac{\partial \check{\mathscr{G}}}{\partial \boldsymbol{\tau}} \cdot \boldsymbol{b}^e \tag{16}$$

where $\boldsymbol{b}^e = \boldsymbol{F}^e \cdot \boldsymbol{F}^{eT}$, $\dot{\lambda}$ is the plastic multiplier and $\mathscr{L}_v$ is the Lie derivative. The formulation was proposed by Simo (1992), whose work is fundamental to understand how the finite strain return mapping can be brought back to a small strain one. The Simo's formulation was proposed to numerically solve finite strain elastoplastic model in the space of principal stress and strain, and in this work is used to formulate an algorithm in the space of two-invariants.

By assuming isotropy, the elastic left Cauchy-Green tensor $\boldsymbol{b}^e$ and the Kirchhoff stress tensor $\boldsymbol{\tau}$ can be spectrally decomposed as

$$\boldsymbol{b}^e = \sum_{A=1}^{3}(\lambda_A^e)^2 \boldsymbol{n}^{(A)} \otimes \boldsymbol{n}^{(A)}; \qquad \boldsymbol{\tau} = \sum_{A=1}^{3} \tau_A \boldsymbol{n}^{(A)} \otimes \boldsymbol{n}^{(A)}. \tag{17}$$

In the context of finite deformations, the *Trial* elastic left Cauchy-Green tensor is given by

$$\boldsymbol{b}^{e\,Tr} = \boldsymbol{f} \cdot \boldsymbol{b}_n^e \cdot \boldsymbol{f}^T, \tag{18}$$

where $\boldsymbol{b}_n^e$ is the elastic left Cauchy-Green tensor and $\boldsymbol{f} = \partial \boldsymbol{x}/\partial \boldsymbol{x}_n$ is the relative deformation gradient with respect to the deformed configuration at time t_n. In spectral form and in the space of the principal elastic logarithmic stretches, the discretized flow rule, obtained by integrating the Lie derivative in Eq. (16), reads

$$\epsilon_A^e = \epsilon_A^{e\,Tr} - \Delta\gamma \frac{\partial \hat{\mathscr{G}}}{\partial \tau_A}. \tag{19}$$

where $\epsilon_A^e = \ln(\lambda_A^e) = \frac{1}{2}\ln(\bar{\lambda}_A^e)$.

Summarizing, in order to compute the updated stress tensor $\boldsymbol{\tau}$, the crucial task is the solution of the non-linear system given by Eq. (19) along with the fulfillment of the plastic condition

$$\boldsymbol{r}(\boldsymbol{x}) = \begin{Bmatrix} \epsilon_A^e - \epsilon_A^{e\,Tr} + \Delta\lambda \frac{\partial \hat{\mathscr{G}}}{\partial \tau_A} \\ \hat{\mathscr{F}}(\tau_A, \boldsymbol{\xi}) \end{Bmatrix} = \boldsymbol{0}; \qquad \boldsymbol{x} = \begin{Bmatrix} \epsilon_A^e \\ \Delta\lambda \end{Bmatrix}; \qquad A = 1, 2, 3. \tag{20}$$

The algorithmic tangent tensor $\boldsymbol{\alpha}$ in Eq. (14), required for the numerical solution of the linear momentum balance equation, is obtained by using the spectral

Implicit elastic predictor/return mapping algorithm for finite strain

```
1. Compute elastic deformation predictor: $\boldsymbol{b}^{e\,Tr} = \boldsymbol{f}_{n+1} \cdot \boldsymbol{b}^e_n \cdot \boldsymbol{f}^T_{n+1}$
2. Perform spectral decomposition: $\boldsymbol{b}^{e\,Tr} = (\lambda_A^{e\,Tr})^2 \boldsymbol{n}^{Tr\,(A)} \otimes \boldsymbol{n}^{Tr\,(A)}$.
3. Compute principal elastic logarithmic strain: $\epsilon_A^{Tr} = \ln(\lambda_A^{e\,Tr})$.
4. Compute elastic stress predictor $\tau_A^{Tr} = \partial\hat{\Psi}(\epsilon_A^{e\,Tr})/\partial\epsilon_A^{e\,Tr}$
5. Check if yielding: $\hat{\mathscr{F}}(\tau_A^{Tr}, \boldsymbol{\xi}_n) \geq 0$?
     No: elastic step. Set $\epsilon^e_A \equiv \epsilon_A^{e\,Tr}$, $\tau_A \equiv \tau_A^{Tr}$, $\boldsymbol{\xi} \equiv \boldsymbol{\xi}_n$, $\bar{\boldsymbol{\xi}} \equiv \bar{\boldsymbol{\xi}}_n$.
     Yes: plastic step. Solve Eq. (20) and compute $\epsilon^e_A$, $\tau_A$, $\boldsymbol{\xi}$, $\bar{\boldsymbol{\xi}}$.
6. Get elastic strain $\boldsymbol{\epsilon}^e$ and stress $\boldsymbol{\tau}$ tensors from $\epsilon^e_A$ and $\tau_A$.
7. Compute consistent tangent operator $a_{AB}$ and $\mathscr{A}$ with Eq. (21) and (14).
8. Compute and store left elastic Cauchy-Green tensor:
     $\boldsymbol{b^e} = \sum_{A=1}^{3} (\exp(\epsilon^e_A))^2 \boldsymbol{n}^{Tr\,(A)} \otimes \boldsymbol{n}^{Tr\,(A)}$.
```

Table 3: Numerical procedure to compute the updated stress state and the consistent tangent operator at the element level for finite strain elastoplasticity.

decomposition previously presented and, in agreement with (Ogden, 1997; Borja et al., 2003), reads

$$\begin{aligned}\boldsymbol{\alpha} = & \sum_{A=1}^{3}\sum_{B=1}^{3} a_{AB}\boldsymbol{m}^{(A)} \otimes \boldsymbol{m}^{(B)} \\ & + \sum_{A=1}^{3}\sum_{B\neq A} \left(\frac{\tau_B - \tau_A}{\bar{\lambda}_B^{e^{Tr}} - \bar{\lambda}_A^{e^{Tr}}}\right)\left(\bar{\lambda}_B^{e^{Tr}}\boldsymbol{m}^{(AB)} \otimes \boldsymbol{m}^{(AB)} + \bar{\lambda}_A^{e^{Tr}}\boldsymbol{m}^{(AB)} \otimes \boldsymbol{m}^{(BA)}\right)\end{aligned} \tag{21}$$

where $a_{AB} = \partial\tau_A/\partial\epsilon_B^{e^{Tr}}$, $2\epsilon_B^{e^{Tr}} = \ln(\bar{\lambda}_B^{e^{Tr}})$ and $\boldsymbol{m}^{(AB)} = \boldsymbol{n}^{(A)} \otimes \boldsymbol{n}^{B}$.

The complete procedure to compute the update state of the stress $\boldsymbol{\tau}$ and the consistent tangent operator $\mathscr{A}$ is summarized in Table 3. It is fundamental to observe that the finite strain assumption leads to the same structure of the algorithm, replacing the principal small strain with the elastic logarithmic stretches and the Cauchy stress with the Kirchhoff one.

3. Return mapping algorithm in two-invariants space

As discussed in the Introduction, many elastoplastic laws are formulated in the space defined by the volumetric and deviatoric invariants. Hence, the return mapping algorithm presented in the previous section for small and finite strain, respectively by means of Eqs. (10) and (20), can be further simplified by introducing the strain and stress invariants defined in Eqs. (1) and (2), such that

$$\boldsymbol{\epsilon}^e = \frac{1}{3}\epsilon_v^e \boldsymbol{\delta} + \sqrt{\frac{3}{2}}\epsilon_s^e \hat{\boldsymbol{n}}; \qquad \boldsymbol{\varsigma} = P\boldsymbol{\delta} + \sqrt{\frac{2}{3}}Q\hat{\boldsymbol{n}}, \tag{22}$$

with $\hat{\boldsymbol{n}} = \boldsymbol{e}^e / \|\boldsymbol{e}^e\|$. Hence, Eqs. (10) and (20) can be rewritten in terms of volumetric and deviatoric invariants, leading to a scalar return mapping algorithm

$$\boldsymbol{r}(\boldsymbol{x}) = \begin{Bmatrix} \epsilon_v^e - \epsilon_v^{e\,Tr} + \Delta\lambda \partial_P \mathscr{G} \\ \epsilon_s^e - \epsilon_s^{e\,Tr} + \Delta\lambda \partial_Q \mathscr{G} \\ \mathscr{F} \end{Bmatrix}; \qquad \boldsymbol{x} = \begin{Bmatrix} \epsilon_v^e \\ \epsilon_s^e \\ \Delta\gamma \end{Bmatrix}, \tag{23}$$

with $\partial_P \mathscr{G} = \frac{\partial \mathscr{G}}{\partial P}$ and $\partial_Q \mathscr{G} = \frac{\partial \mathscr{G}}{\partial Q}$. In the most general case,

$$\mathscr{F} = \mathscr{F}(P, Q, \xi_1, ..., \xi_\alpha) \tag{24}$$

with ξ_i possible stress-like hardening parameters and

$$\mathscr{G} = \mathscr{G}(P, Q, \bar{\xi}_1, ..., \bar{\xi}_{\bar{\alpha}}), \tag{25}$$

with $\bar{\xi}_i$ possible stress-like parameters that control the evolution of the plastic potential.

By assuming that the parameters ξ_i and $\bar{\xi}_i$ depend on the accumulated deformations, it is always possible to express these functions in the following form

$$\xi_i = \xi_i(\epsilon_v^e, \epsilon_v^{e\,Tr}, \epsilon_s^e, \epsilon_s^{e\,Tr}); \qquad \bar{\xi}_i = \bar{\xi}_i(\epsilon_v^e, \epsilon_v^{e\,Tr}, \epsilon_s^e, \epsilon_s^{e\,Tr}). \tag{26}$$

Finally, in order to further generalize the formulation, let's consider a class of two-invariants elastic potential function of the form

$$\Psi = \Psi(\epsilon_v^e, \epsilon_s^e), \tag{27}$$

Elastoplastic model in two-invariants space
1. Stored energy: $\Psi = \Psi(\epsilon_v^e, \epsilon_s^e) \Longrightarrow P = P(\epsilon_v^e, \epsilon_s^e)$ and $Q = Q(\epsilon_v^e, \epsilon_s^e)$;
2. Yield function: $\mathscr{F} = \mathscr{F}(P, Q, \xi_1, ..., \xi_\alpha)$;
3. Hardening law: $\xi_i = \xi_i(\epsilon_v^e, {\epsilon_v^e}^{Tr}, \epsilon_s^e, {\epsilon_s^e}^{Tr})$ for $i = 1, ..., \alpha$;
4. Plastic potential: $\mathscr{G} = \mathscr{G}(P, Q, \bar{\xi}_1, ..., \bar{\xi}_{\bar{\alpha}})$;
5. Plastic potential parameters: $\bar{\xi}_i = \bar{\xi}_i(\epsilon_v^e, {\epsilon_v^e}^{Tr}, \epsilon_s^e, {\epsilon_s^e}^{Tr})$ for $i = 1, ..., \bar{\alpha}$.

Table 4: General set of equations for an elastoplastic model defined in the two-invariants space.

which describes a general hyperelastic constitutive relation. Therefore, the relation between stress and strain invariants in the elastic regime directly comes from the derivation of the stored energy function with respect to the deformation, i.e.

$$P = \frac{\partial \Psi(\epsilon_v^e, \epsilon_s^e)}{\partial \epsilon_v^e}; \qquad\qquad Q = \frac{\partial \Psi(\epsilon_v^e, \epsilon_s^e)}{\partial \epsilon_s^e}. \tag{28}$$

This formulation allows a general non-linear behaviour in the elastic regime. By summarizing and reordering the equations, the most general elastoplastic model in a two-invariants space requires the characterization of the functions reported in Table 4.

The definition of the return mapping in the space of the two-invariants allows to further simplify the algorithm at the Gauss point level proposed in Tables 2 and 3. The modified algorithm is reported in Table 5, where the same enumeration has been adopted for sake of clarity. It is important to note that the direction vector of the principal deviatoric elastic strains, $\hat{\boldsymbol{n}}$, is obtained via its trial value, $\hat{\boldsymbol{n}}^{Tr}$. Furthermore, the principal directions $n^{(A)} (A = 1, 2, 3)$ are obtained via the relation $\boldsymbol{n}^{Tr(A)} = \boldsymbol{n}^{(A)}$, originating from the assumption of isotropy.

Writing the return mapping algorithm in the space of the two-invariants simplifies the non-linear system of equations from four to three equations/unknowns, as well as the computation of the tangent operator $\boldsymbol{a}^{ep}$. The solution of the non-

```
Implicit elastic predictor/return mapping algorithm
for small/finite strain in two-invariants space.

1. Compute elastic deformation predictor.
2. Perform spectral decomposition.
3(a). Compute principal elastic strain: $\epsilon_A^{Tr}$.
  3(b). Compute elastic strain invariants ${\epsilon_v^e}^{Tr}$ and ${\epsilon_s^e}^{Tr}$ according to Eq. (1).
  4. Compute elastic stress predictor $P^{Tr}$ and $Q^{Tr}$ according to Eq. (28).
  5. Check if yielding: $\mathscr{F}(P^{Tr}, Q^{Tr}, \boldsymbol{\xi}_n) \geq 0$?
    No: elastic step. Set $(\epsilon_v^e, \epsilon_s^e) \equiv ({\epsilon_v^e}^{Tr}, {\epsilon_s^e}^{Tr})$, $(P, Q) \equiv (P^{Tr}, Q^{Tr})$, $\boldsymbol{\xi} \equiv \boldsymbol{\xi}_n$, $\bar{\boldsymbol{\xi}} \equiv \bar{\boldsymbol{\xi}}_n$.
    Yes: plastic step. Solve Eq. (23) and compute $(\epsilon_v^e, \epsilon_s^e)$, $(P, Q)$, $\boldsymbol{\xi}$, $\bar{\boldsymbol{\xi}}$.
  6(a). Get principal elastic strain $\epsilon_A^e$ and principal stress $\sigma_A$ (or $\tau_A$) from $(\epsilon_v^e, \epsilon_s^e)$
        and $(P, Q)$ with Eq. (22).
6(b). Get elastic strain $\boldsymbol{\epsilon}^e$ and stress $\boldsymbol{\sigma}$ (or $\boldsymbol{\tau}$) tensors from $\epsilon_A^e$ and $\sigma_A$ (or $\tau_A$).
7. Compute consistent tangent operator $a_{AB}$.
8. Compute and store elastic variables.
```

Table 5: Numerical procedure to compute the updated stress state and the consistent tangent operator at the element level in the two-invariants space.

linear system in Eq. (23) and the computation of the tangent operator $\boldsymbol{a}^{ep}$ will be discussed in detail in the next section, proposing a general algorithm to fulfill the above tasks for a fully general elastoplastic model defined as in Table 4.

4. General form to solve two-invariants elastoplasticity

4.1. General derivative of the functions

In order to define a general algorithm for the solution of the elastoplastic formulation presented in the previous section, it is convenient to introduce the following matrices, which will help to write the required operators in a compact form

$$\boldsymbol{D}^e = \begin{bmatrix} D^e_{11} & D^e_{12} \\ D^e_{21} & D^e_{22} \end{bmatrix} = \begin{bmatrix} \partial_{\epsilon^e_v} P & \partial_{\epsilon^e_s} P \\ \partial_{\epsilon^e_v} Q & \partial_{\epsilon^e_s} Q \end{bmatrix} ; \tag{29}$$

$$\boldsymbol{E}^{(Tr)} = \begin{bmatrix} D^e_{11} & D^e_{12} \\ D^e_{21} & D^e_{22} \\ \partial_{\epsilon^{e\,(Tr)}_v} \xi_1 & \partial_{\epsilon^{e\,(Tr)}_s} \xi_1 \\ \vdots & \vdots \\ \partial_{\epsilon^{e\,(Tr)}_v} \xi_\alpha & \partial_{\epsilon^{e\,(Tr)}_s} \xi_\alpha \end{bmatrix} ; \quad \bar{\boldsymbol{E}}^{(Tr)} = \begin{bmatrix} D^e_{11} & D^e_{12} \\ D^e_{21} & D^e_{22} \\ \partial_{\epsilon^{e\,(Tr)}_v} \bar{\xi}_1 & \partial_{\epsilon^{e\,(Tr)}_s} \bar{\xi}_1 \\ \vdots & \vdots \\ \partial_{\epsilon^{e\,(Tr)}_v} \bar{\xi}_{\bar{\alpha}} & \partial_{\epsilon^{e\,(Tr)}_s} \bar{\xi}_{\bar{\alpha}} \end{bmatrix} ; \tag{30}$$

and

$$\boldsymbol{F} = \begin{bmatrix} \partial_P \mathscr{F} \\ \partial_Q \mathscr{F} \\ \partial_{\xi_1} \mathscr{F} \\ \vdots \\ \partial_{\xi_\alpha} \mathscr{F} \end{bmatrix} ; \qquad \boldsymbol{G} = \begin{bmatrix} \partial_P \mathscr{G} \\ \partial_Q \mathscr{G} \\ \partial_{\bar{\xi}_1} \mathscr{G} \\ \vdots \\ \partial_{\bar{\xi}_{\bar{\alpha}}} \mathscr{G} \end{bmatrix} ; \tag{31}$$

$$\boldsymbol{H} = \begin{bmatrix} \partial_{PP}\mathscr{G} & \partial_{PQ}\mathscr{G} & \partial_{P\bar{\xi}_1}\mathscr{G} & \dots & \partial_{P\bar{\xi}_{\bar{\alpha}}}\mathscr{G} \\ \partial_{QP}\mathscr{G} & \partial_{QQ}\mathscr{G} & \partial_{Q\bar{\xi}_1}\mathscr{G} & \dots & \partial_{Q\bar{\xi}_{\bar{\alpha}}}\mathscr{G} \\ \partial_{\bar{\xi}_1 P}\mathscr{G} & \partial_{\bar{\xi}_1 Q}\mathscr{G} & \partial_{\bar{\xi}_1\bar{\xi}_1}\mathscr{G} & \dots & \partial_{\bar{\xi}_1\bar{\xi}_{\bar{\alpha}}}\mathscr{G} \\ \vdots & \vdots & \vdots & \ddots & \vdots \\ \partial_{\bar{\xi}_{\bar{\alpha}} P}\mathscr{G} & \partial_{\bar{\xi}_{\bar{\alpha}} Q}\mathscr{G} & \partial_{\bar{\xi}_{\bar{\alpha}}\bar{\xi}_1}\mathscr{G} & \dots & \partial_{\bar{\xi}_{\bar{\alpha}}\bar{\xi}_{\bar{\alpha}}}\mathscr{G}, \end{bmatrix} \tag{32}$$

with the matrices $\boldsymbol{E}^{(Tr)}$,$\bar{\boldsymbol{E}}^{(Tr)}$, $\boldsymbol{H}$ of dimension $(2+\alpha) \times 2$, $(2+\bar{\alpha}) \times 2$, $(2+\bar{\alpha}) \times (2+\bar{\alpha})$ respectively and the vectors $\boldsymbol{F}$, $\boldsymbol{G}$ of $(2+\alpha)$ and $(2+\bar{\alpha})$ elements, respectively. These newly defined matrices and vectors will be used in the following sections.

4.2. Solution of the non-linear system of Eq. (23)

To solve the non-linear system of Eq. (23) it is necessary to dissipate the residual vector $\boldsymbol{r}$ by finding the solution vector $\boldsymbol{x}^*$ using Newton's method

$$\boldsymbol{x}^{k+1} = \boldsymbol{x}^k + \delta\boldsymbol{x}^k; \qquad -\boldsymbol{A}^k\delta\boldsymbol{x}^k = \boldsymbol{r}^k; \qquad \boldsymbol{A}^k = \frac{\partial \boldsymbol{r}^k}{\partial \boldsymbol{x}^k};\ k \leftarrow k+1, \tag{33}$$

where k plays the role of an iteration counter.

The 3×3 Jacobian matrix $\boldsymbol{A}^k$ in Eq. (33) for return mapping iteration is obtained by differentiating the component of $\boldsymbol{r}$ with respect to the variables $\boldsymbol{x}$ defined in Eq. (23). For sake of simplicity, the superscript k denoting the value at k-th iteration is suppressed in the following derivation. Therefore the general form of the matrix $\boldsymbol{A}$ is

$$\boldsymbol{A} = \begin{bmatrix} 1 + \Delta\gamma(H_{1a}\bar{E}_{a1}) & \Delta\gamma(H_{1a}\bar{E}_{a2}) & G_1 \\ \Delta\gamma(H_{2a}\bar{E}_{a1}) & 1 + \Delta\gamma(H_{2a}\bar{E}_{a2}) & G_2 \\ F_b E_{b1} & F_b E_{b2} & 0 \end{bmatrix} \tag{34}$$

for $a = 1, ..., (2+\alpha)$ and $b = 1, ..., (2+\bar{\alpha})$. Hence, once the matrices in Section 4.1 have been defined, the computation of the tangent operator $\boldsymbol{A}$ and the solution of the system in Eq. (23) follows straightforward, whatever the functions defined in Table 4 are.

4.3. Derivation of the consistent tangent operator $\boldsymbol{a}$

In this section an expression for the tangential moduli matrix $\boldsymbol{a}$

$$\boldsymbol{a} := \frac{\partial \boldsymbol{\tau}}{\partial \boldsymbol{\epsilon}^{e\;Tr}} \tag{35}$$

is derived, that can be used in the elastoplastic regime. By taking advantage of the decomposition of Eq. (22), the following strain-derivative holds

$$\boldsymbol{a}^{ep} = \boldsymbol{\delta} \otimes \frac{\partial P}{\partial \boldsymbol{\epsilon}^{e\;Tr}} + \sqrt{\frac{2}{3}}\hat{\boldsymbol{n}} \otimes \frac{\partial Q}{\partial \boldsymbol{\epsilon}^{e\;Tr}} + \sqrt{\frac{2}{3}}Q\frac{\partial \hat{\boldsymbol{n}}}{\partial \boldsymbol{\epsilon}^{e\;Tr}} \tag{36}$$

where

$$\frac{\partial \hat{\boldsymbol{n}}}{\partial \boldsymbol{\epsilon}^{e\;Tr}} = \frac{1}{\|\boldsymbol{e}^{e\;Tr}\|}\left(\boldsymbol{I} - \frac{1}{3}\boldsymbol{\delta} \otimes \boldsymbol{\delta} - \hat{\boldsymbol{n}} \otimes \hat{\boldsymbol{n}}\right). \tag{37}$$

The material tangent operator can be written again as function of the two-invariants as

$$\begin{aligned}\boldsymbol{a}^{ep} = \boldsymbol{\delta} \otimes \left(D^e_{11}\frac{\partial \epsilon^e_v}{\partial \boldsymbol{\epsilon}^{e\;Tr}} + D^e_{12}\frac{\partial \epsilon^e_s}{\partial \boldsymbol{\epsilon}^{e\;Tr}}\right) + \sqrt{\frac{2}{3}}\hat{\boldsymbol{n}} \otimes \left(D^e_{21}\frac{\partial \epsilon^e_v}{\partial \boldsymbol{\epsilon}^{e\;Tr}} + D^e_{22}\frac{\partial \epsilon^e_s}{\partial \boldsymbol{\epsilon}^{e\;Tr}}\right) + \\ \frac{2Q}{3\epsilon^{e\;Tr}_s}\left(\boldsymbol{I} - \frac{1}{3}\boldsymbol{\delta} \otimes \boldsymbol{\delta} - \hat{\boldsymbol{n}} \otimes \hat{\boldsymbol{n}}\right).\end{aligned} \tag{38}$$

The task is then reduced to determine the strain derivatives of the invariants ϵ^e_v and ϵ^e_s, which is obtained from the first two equations reported in (23)

$$\frac{\partial \epsilon^e_v}{\partial \boldsymbol{\epsilon}^{e\;Tr}} = \frac{\partial}{\partial \boldsymbol{\epsilon}^{e\;Tr}}\left(\epsilon^{e\;Tr}_v - \Delta\gamma\frac{\partial \mathscr{G}}{\partial P}\right); \tag{39a}$$

$$\frac{\partial \epsilon^e_s}{\partial \boldsymbol{\epsilon}^{e\;Tr}} = \frac{\partial}{\partial \boldsymbol{\epsilon}^{e\;Tr}}\left(\epsilon^{e\;Tr}_s - \Delta\gamma\frac{\partial \mathscr{G}}{\partial Q}\right). \tag{39b}$$

In order to reduce the derivatives to their lowest order, we expand Eqs. (39a, 39b). In the expansion we will need the following strain derivative of ξ_i and $\bar{\xi}_i$

$$\frac{\partial \xi_i}{\partial \boldsymbol{\epsilon}^{e\;Tr}} = \frac{\partial \xi_i}{\partial \epsilon^e_v}\frac{\partial \epsilon^e_v}{\partial \boldsymbol{\epsilon}^{e\;Tr}} + \frac{\partial \xi_i}{\partial \epsilon^{e\;Tr}_v}\frac{\partial \epsilon^{e\;Tr}_v}{\partial \boldsymbol{\epsilon}^{e\;Tr}} + \frac{\partial \xi_i}{\partial \epsilon^e_s}\frac{\partial \epsilon^e_s}{\partial \boldsymbol{\epsilon}^{e\;Tr}} + \frac{\partial \xi_i}{\partial \epsilon^{e\;Tr}_s}\frac{\partial \epsilon^{e\;Tr}_s}{\partial \boldsymbol{\epsilon}^{e\;Tr}} \tag{40}$$

$$= E_{i1}\frac{\partial \epsilon^e_v}{\partial \boldsymbol{\epsilon}^{e\;Tr}} + E^{Tr}_{i1}\boldsymbol{\delta} + E_{i2}\frac{\partial \epsilon^e_s}{\partial \boldsymbol{\epsilon}^{e\;Tr}} + E^{Tr}_{i2}\sqrt{\frac{2}{3}}\hat{\boldsymbol{n}} \tag{41}$$

$$
\begin{aligned}
\frac{\partial \bar{\xi}_i}{\partial \boldsymbol{\epsilon}^{e\,Tr}} &= \frac{\partial \bar{\xi}_i}{\partial \epsilon_v^e}\frac{\partial \epsilon_v^e}{\partial \boldsymbol{\epsilon}^{e\,Tr}} + \frac{\partial \bar{\xi}_i}{\partial \epsilon_v^{e\,Tr}}\frac{\partial \epsilon_v^{e\,Tr}}{\partial \boldsymbol{\epsilon}^{e\,Tr}} + \frac{\partial \bar{\xi}_i}{\partial \epsilon_s^e}\frac{\partial \epsilon_s^e}{\partial \boldsymbol{\epsilon}^{e\,Tr}} + \frac{\partial \bar{\xi}_i}{\partial \epsilon_s^{e\,Tr}}\frac{\partial \epsilon_s^{e\,Tr}}{\partial \boldsymbol{\epsilon}^{e\,Tr}} \quad (42)\\
&= \bar{E}_{i1}\frac{\partial \epsilon_v^e}{\partial \boldsymbol{\epsilon}^{e\,Tr}} + \bar{E}_{i1}^{Tr}\boldsymbol{\delta} + \bar{E}_{i2}\frac{\partial \epsilon_s^e}{\partial \boldsymbol{\epsilon}^{e\,Tr}} + \bar{E}_{i2}^{Tr}\sqrt{\frac{2}{3}}\hat{\boldsymbol{n}} \quad (43)
\end{aligned}
$$

The expansion of Eqs. (39a, 39b) becomes

$$
b_{11}\frac{\partial \epsilon_v^e}{\partial \boldsymbol{\epsilon}^{e\,Tr}} + b_{12}\frac{\partial \epsilon_s^e}{\partial \boldsymbol{\epsilon}^{e\,Tr}} = c_{11}\boldsymbol{\delta} + c_{12}\sqrt{\frac{2}{3}}\hat{\boldsymbol{n}} - \left(\frac{\partial \mathscr{G}}{\partial P}\right)\left(\frac{\partial \Delta\gamma}{\partial \boldsymbol{\epsilon}^{e\,Tr}}\right) \quad (44a)
$$

$$
b_{21}\frac{\partial \epsilon_v^e}{\partial \boldsymbol{\epsilon}^{e\,Tr}} + b_{22}\frac{\partial \epsilon_s^e}{\partial \boldsymbol{\epsilon}^{e\,Tr}} = c_{21}\boldsymbol{\delta} + c_{22}\sqrt{\frac{2}{3}}\hat{\boldsymbol{n}} - \left(\frac{\partial \mathscr{G}}{\partial Q}\right)\left(\frac{\partial \Delta\gamma}{\partial \boldsymbol{\epsilon}^{e\,Tr}}\right) \quad (44b)
$$

where

$$
b_{ij} = \delta_{ij} + \Delta\gamma\left(H_{ia}\bar{E}_{aj}\right) \qquad \text{with } a = 1, ..., (2+\bar{\alpha}) \quad (45a)
$$

$$
c_{ij} = \delta_{ij} - \Delta\gamma\left(H_{ib}\bar{E}_{bj}^{Tr}\right) \qquad \text{with } b = 3, ..., (2+\bar{\alpha}) \quad (45b)
$$

with δ_{ij} the Kronecker delta.

Solving Eqs. (44,44b) simultaneously with Cramer's rule yields

$$
\det(\boldsymbol{b})\frac{\partial \epsilon_v^e}{\partial \boldsymbol{\epsilon}^{e\,Tr}} = l_{11}\boldsymbol{\delta} + l_{12}\sqrt{\frac{2}{3}}\hat{\boldsymbol{n}} - l_{13}\left(\frac{\partial \Delta\gamma}{\partial \boldsymbol{\epsilon}^{e\,Tr}}\right) \quad (46a)
$$

$$
\det(\boldsymbol{b})\frac{\partial \epsilon_s^e}{\partial \boldsymbol{\epsilon}^{e\,Tr}} = l_{21}\boldsymbol{\delta} + l_{22}\sqrt{\frac{2}{3}}\hat{\boldsymbol{n}} - l_{23}\left(\frac{\partial \Delta\gamma}{\partial \boldsymbol{\epsilon}^{e\,Tr}}\right) \quad (46b)
$$

where $\det(\boldsymbol{b}) = b_{11}b_{22} - b_{12}b_{21}$ and

$$
l_{11} = b_{22}c_{11} - b_{12}c_{21} \qquad l_{21} = b_{11}c_{21} - b_{21}c_{11} \quad (47a)
$$

$$
l_{12} = b_{22}c_{12} - b_{12}c_{22} \qquad l_{22} = b_{11}c_{22} - b_{21}c_{12} \quad (47b)
$$

$$
l_{13} = G_1 b_{22} - G_2 b_{12} \qquad l_{23} = G_1 b_{11} - G_2 b_{21} \quad (47c)
$$

The strain-gradient of the plastic multiplier $\left(\frac{\partial \Delta\gamma}{\partial \boldsymbol{\epsilon}^{e\,Tr}}\right)$ is obtained from the overall consistency condition

$$
\frac{\partial \mathscr{F}}{\partial \boldsymbol{\epsilon}^{e\,Tr}} = \frac{\partial \mathscr{F}}{\partial P}\frac{\partial P}{\partial \boldsymbol{\epsilon}^{e\,Tr}} + \frac{\partial \mathscr{F}}{\partial Q}\frac{\partial Q}{\partial \boldsymbol{\epsilon}^{e\,Tr}} + \frac{\partial \mathscr{F}}{\partial \xi_i}\frac{\partial \xi_i}{\partial \boldsymbol{\epsilon}^{e\,Tr}} = 0 \quad (48)
$$

with summation over the index i. Since P, Q and ξ_i are functions of the strain invariants, we can expand Eq. (48) further by the chain rule and use Eq. (40) to obtain

$$\frac{\partial \mathscr{F}}{\partial \boldsymbol{\epsilon}^{e\,Tr}} = d_1 \frac{\partial \epsilon_v^e}{\partial \boldsymbol{\epsilon}^{e\,Tr}} + d_2 \frac{\partial \epsilon_s^e}{\partial \boldsymbol{\epsilon}^{e\,Tr}} + F_b E_{b1}^{Tr} \boldsymbol{\delta} + F_b E_{b2}^{Tr} \sqrt{\frac{2}{3}} \hat{\boldsymbol{n}} = 0 \tag{49}$$

with $b = 3, ..., (2+\alpha)$ where

$$d_1 = F_a E_{a1} \qquad\qquad d_2 = F_a E_{a2} \tag{50}$$

with $a = 1, ..., (2+\alpha)$.

Therefore, by substituting Eqs. (46a, 46b) into Eq. (49) we obtain

$$\frac{\partial \mathscr{F}}{\partial \boldsymbol{\epsilon}^{e\,Tr}} = d_1 \left[l_{11} \boldsymbol{\delta} + l_{12} \sqrt{\frac{2}{3}} \hat{\boldsymbol{n}} - l_{13} \left(\frac{\partial \Delta\gamma}{\partial \boldsymbol{\epsilon}^{e\,Tr}} \right) \right] + d_2 \left[l_{21} \boldsymbol{\delta} + l_{22} \sqrt{\frac{2}{3}} \hat{\boldsymbol{n}} - l_{23} \left(\frac{\partial \Delta\gamma}{\partial \boldsymbol{\epsilon}^{e\,Tr}} \right) \right] + \\ + \det(\boldsymbol{b}) F_b E_{b1}^{Tr} \boldsymbol{\delta} + \det(\boldsymbol{b}) F_b E_{b2}^{Tr} \sqrt{\frac{2}{3}} \hat{\boldsymbol{n}} = 0 \tag{51}$$

with $b = 3, ..., (2+\alpha)$ and solving for $\left(\frac{\partial \Delta\gamma}{\partial \boldsymbol{\epsilon}^{e\,Tr}} \right)$ we get

$$\frac{\partial \Delta\gamma}{\partial \boldsymbol{\epsilon}^{e\,Tr}} = a_1 \boldsymbol{\delta} + a_2 \sqrt{\frac{2}{3}} \hat{\boldsymbol{n}} \tag{52}$$

where

$$a_1 = \left(d_1 l_{11} + d_2 l_{21} + \det(\boldsymbol{b}) F_b E_{b1}^{Tr} \right) / e \tag{53a}$$

$$a_2 = \left(d_1 l_{12} + d_2 l_{22} + \det(\boldsymbol{b}) F_b E_{b2}^{Tr} \right) / e \tag{53b}$$

with $b = 3, ..., (2+\alpha)$ and

$$e = d_1 l_{13} + d_2 l_{23} \tag{54}$$

Finally, by inserting Eq. (52) into Eq. (46) we get

$$\frac{\partial \epsilon_v^e}{\partial \boldsymbol{\epsilon}^{e\,Tr}} = \frac{l_{11} - a_1 l_{13}}{\det(\boldsymbol{b})}\boldsymbol{\delta} + \frac{l_{12} - a_2 l_{13}}{\det(\boldsymbol{b})}\sqrt{\frac{2}{3}}\hat{\boldsymbol{n}} = D_{11}^p \boldsymbol{\delta} + D_{12}^p \sqrt{\frac{2}{3}}\hat{\boldsymbol{n}} \tag{55a}$$

$$\frac{\partial \epsilon_s^e}{\partial \boldsymbol{\epsilon}^{e\,Tr}} = \frac{l_{21} - a_1 l_{23}}{\det(\boldsymbol{b})}\boldsymbol{\delta} + \frac{l_{22} - a_2 l_{23}}{\det(\boldsymbol{b})}\sqrt{\frac{2}{3}}\hat{\boldsymbol{n}} = D_{21}^p \boldsymbol{\delta} + D_{22}^p \sqrt{\frac{2}{3}}\hat{\boldsymbol{n}} \tag{55b}$$

We identify the 2 × 2 matrix $\boldsymbol{D}^p$, with components $(\boldsymbol{D}^p)_{ij} = D_{ij}^p$, as an operator which maps the basis vectors $\boldsymbol{\delta}$ and $\sqrt{2/3}\hat{\boldsymbol{n}}$ onto the derivatives with respect to $\boldsymbol{\epsilon}^{e\,Tr}$ of the elastic strain invariants ϵ_v^e and ϵ_s^e. Consequently, by defining

$$\boldsymbol{D}^{ep} = \boldsymbol{D}^e \boldsymbol{D}^p, \tag{56}$$

the strain gradients of the stress invariants then take the form

$$\frac{\partial P}{\partial \boldsymbol{\epsilon}^{e\,Tr}} = D_{11}^{ep} \boldsymbol{\delta} + D_{12}^{ep} \sqrt{\frac{2}{3}}\hat{\boldsymbol{n}} \tag{57a}$$

$$\frac{\partial Q}{\partial \boldsymbol{\epsilon}^{e\,Tr}} = D_{21}^{ep} \boldsymbol{\delta} + D_{22}^{ep} \sqrt{\frac{2}{3}}\hat{\boldsymbol{n}} \tag{57b}$$

Substituting Eq. (57) into Eq. (38) then yields the desired consistent tangent modulus

$$\boldsymbol{a}^{ep} = \left(D_{11}^{ep} - \frac{2Q}{9\epsilon_s^e}\right)\boldsymbol{\delta}\otimes\boldsymbol{\delta} + \sqrt{\frac{2}{3}}D_{12}^{ep}\boldsymbol{\delta}\otimes\hat{\boldsymbol{n}} + \sqrt{\frac{2}{3}}D_{21}^{ep}\hat{\boldsymbol{n}}\otimes\boldsymbol{\delta} + \frac{2Q}{3\epsilon_s^{e\,Tr}}\left(\boldsymbol{I} - \hat{\boldsymbol{n}}\otimes\hat{\boldsymbol{n}}\right) + \frac{2}{3}D_{22}^{ep}\hat{\boldsymbol{n}}\otimes\hat{\boldsymbol{n}} \tag{58}$$

It is hence sufficient to compute the matrices $\boldsymbol{D}^e$, $\boldsymbol{E}^{(Tr)}$, $\bar{\boldsymbol{E}}^{(Tr)}$, $\boldsymbol{F}$, $\boldsymbol{G}$ and $\boldsymbol{H}$ for the specific set of adopted equations, and the operator $\boldsymbol{A}$ and $\boldsymbol{a}^{ep}$ follow straightforward.

In the next section this procedure will be applied to two classical elastoplastic models.

Drucker-Prager model
1. Stored energy: $\Psi = \Psi(\epsilon_v^e, \epsilon_s^e) = \frac{1}{2}K\epsilon_v^{e\,2} + \frac{3}{2}G\epsilon_s^{e\,2} \Longrightarrow$
$P = K\epsilon_v^e$ and $Q = 3G\epsilon_s^e$;
2. Yield function: $\mathscr{F} = Q - mP - c = 0$;
3. Hardening law: $\xi_1 = c = c_0 + h\epsilon_s^p$
with $\epsilon_s^p = \epsilon_s^{e\,Tr} + \epsilon_{s,n}^p - \epsilon_s^e$, $\alpha = 1$;
4. Plastic potential: $\mathscr{G} = Q - \bar{m}P - \bar{c} = 0$;
5. Plastic potential parameters: *no parameters*, $\bar{\alpha} = 0$

Table 6: Equations of the Drucker-Prager model.

5. Numerical examples

5.1. Introduction and constitutive laws

This section shows how the developed framework can be used for implementing two elastoplastic materials, namely the Drucker-Prager (DP) and the Modified Cam-Clay (MCC) laws. The choice to apply the proposed approach to two simple and very common elastoplastic laws is to make it more understandable for the reader; obviously, this approach can be easily applied to every other constitutive model. Indeed, the goal of this section is not to focus on the specific results in term of displacements or strain/stress, but rather to show the robustness of the framework.

The equations characterizing the non-associated Drucker-Prager model (Drucker & Prager, 1952) with linear hardening are summarized in Table 6. The model is defined by a linear isotropic elastic law, a yield function (graphically represented in Fig. 1) which depends on the parameters m and c (associated to the friction angle and the cohesion of the material, respectively), a linear hardening law depending on the accumulated plastic deviatoric strain and a linear plastic potential depending on the parameter $\bar{m}$ (associated to the dilatancy angle).

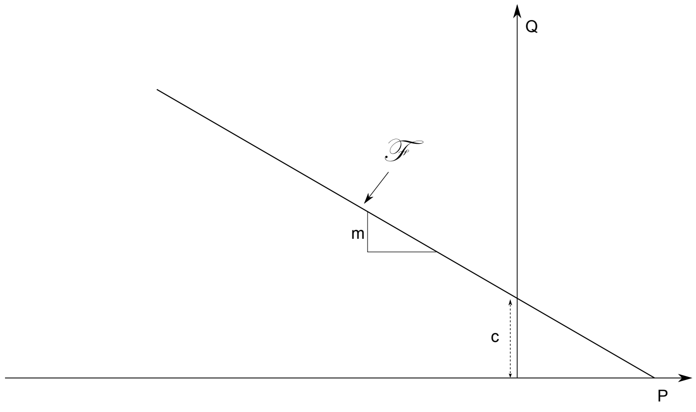

Figure 1: Drucker-Prager yield surface.

The matrices that will give the operators $\boldsymbol{A}$ and $\boldsymbol{a}^{ep}$ are calculated as follows

$$\boldsymbol{D}^e = \begin{bmatrix} D^e_{11} & D^e_{12} \\ D^e_{21} & D^e_{22} \end{bmatrix} = \begin{bmatrix} K & 0 \\ 0 & 3G \end{bmatrix}; \tag{59}$$

$$\boldsymbol{E} = \begin{bmatrix} K & 0 \\ 0 & 3G \\ 0 & -h \end{bmatrix}; \qquad \boldsymbol{E}^{Tr} = \begin{bmatrix} K & 0 \\ 0 & 3G \\ 0 & 2h \end{bmatrix}; \tag{60}$$

$$\bar{\boldsymbol{E}} = \begin{bmatrix} K & 0 \\ 0 & 3G \end{bmatrix}; \qquad \bar{\boldsymbol{E}}^{Tr} = \begin{bmatrix} K & 0 \\ 0 & 3G \end{bmatrix}; \tag{61}$$

and

$$\boldsymbol{F} = \begin{bmatrix} -m \\ 1 \\ -1 \end{bmatrix}; \qquad \boldsymbol{G} = \begin{bmatrix} -\bar{m} \\ 1 \end{bmatrix}; \tag{62}$$

$$\boldsymbol{H} = \begin{bmatrix} 0 & 0 \\ 0 & 0 \end{bmatrix} \tag{63}$$

Modified Cam-Clay model
1. Stored energy: $\Psi = \Psi(\epsilon_v^e, \epsilon_s^e) = \tilde{\psi}(\epsilon_v^e) + \frac{3}{2}\mu^e \epsilon_s^{e2}$
with $\tilde{\psi}(\epsilon_v^e) = -P_0 k \exp(\Omega)$; $\Omega = -(\epsilon_v^e - \epsilon_{v0}^e)/k \Longrightarrow$
$P = P_0 \exp(\Omega)\left[1 + \frac{3\alpha}{2k}(\epsilon_s^e)^2\right]\epsilon_v^e$ and $Q = 3(\mu_0 - \alpha P_0 \exp\Omega)\epsilon_s^e$;
2. Yield function: $\mathscr{F} = \frac{Q^2}{M^2} + P(P - P_c) = 0$;
3. Hardening law: $\xi_1 = P_c = P_{c,n}\exp[-\Theta(\epsilon_v^{e\,Tr} - \epsilon_v^e)]$, $\alpha = 1$;
4. Plastic potential: $\mathscr{G} = \mathscr{F} = \frac{Q^2}{M^2} + P(P - P_c) = 0$;
5. Plastic potential parameters: $\bar{\xi}_1 = P_c = P_{c,n}\exp[-\Theta(\epsilon_v^{e\,Tr} - \epsilon_v^e)]$, $\bar{\alpha} = 1$;

Table 7: Equations of the Modified Cam-Clay model.

with the matrices $\boldsymbol{E}^{(Tr)}$, $\bar{\boldsymbol{E}}^{(Tr)}$, $\boldsymbol{H}$ of dimension 3×2, 2×2 and 2×2 respectively, the vectors $\boldsymbol{F}$ and $\boldsymbol{G}$ have 3 and 2 elements, respectively.
Once these matrices and vectors have been defined, the algorithm builds up all the remaining part of the work.
A second example of constitutive law is the Modified Cam-Clay model (Roscoe & Burland, 1968), here in the extended version proposed by Borja & Tamagnini (1998). The set of equations that characterizes the constitutive law are summarized in Table 7. Hence, the matrices that will give the operators $\boldsymbol{A}$ and $\boldsymbol{a}^{ep}$

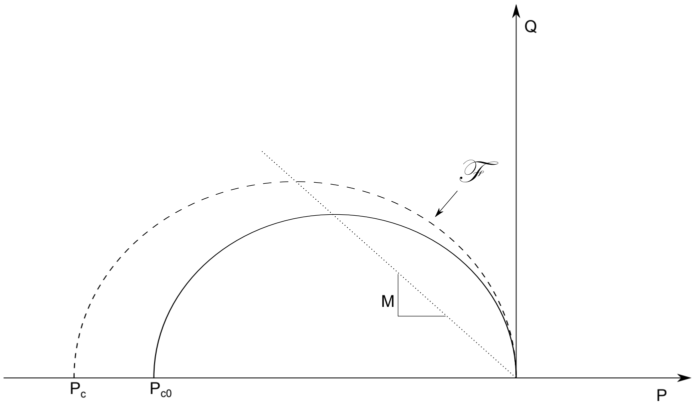

Figure 2: Modified Cam-Clay yield surface.

are

$$\boldsymbol{D}^e = \begin{bmatrix} D^e_{11} & D^e_{12} \\ D^e_{21} & D^e_{22} \end{bmatrix} = \begin{bmatrix} -\frac{P_0}{k}\exp(\Omega)\left[1+\frac{3\alpha}{2k}(\epsilon^e_s)^2\right] & \frac{3P_0\alpha\epsilon^e_s}{k}\exp(\Omega) \\ \frac{3P_0\alpha\epsilon^e_s}{k}\exp(\Omega) & 3(\mu_0-\alpha P_0\exp\Omega)\epsilon^e_s \end{bmatrix}; \tag{64}$$

$$\boldsymbol{E} = \begin{bmatrix} D^e_{11} & D^e_{12} \\ D^e_{21} & D^e_{22} \\ \Theta P_c & 0 \end{bmatrix}; \qquad \boldsymbol{E}^{Tr} = \begin{bmatrix} D^e_{11} & D^e_{12} \\ D^e_{21} & D^e_{22} \\ -\Theta P_c & 0 \end{bmatrix}; \tag{65}$$

$$\bar{\boldsymbol{E}} = \begin{bmatrix} D^e_{11} & D^e_{12} \\ D^e_{21} & D^e_{22} \\ \Theta P_c & 0 \end{bmatrix}; \qquad \bar{\boldsymbol{E}}^{Tr} = \begin{bmatrix} D^e_{11} & D^e_{12} \\ D^e_{21} & D^e_{22} \\ -\Theta P_c & 0 \end{bmatrix}; \tag{66}$$

and

$$\boldsymbol{F} = \begin{bmatrix} 2P-P_c \\ 2Q/M^2 \\ -P \end{bmatrix}; \qquad \boldsymbol{G} = \begin{bmatrix} 2P-P_c \\ 2Q/M^2 \\ -P \end{bmatrix}; \tag{67}$$

$$\boldsymbol{H} = \begin{bmatrix} 2 & 0 & -1 \\ 0 & 2/M^2 & 0 \\ -1 & 0 & 0 \end{bmatrix} \tag{68}$$

with matrices $\boldsymbol{E}^{(Tr)}$, $\bar{\boldsymbol{E}}^{(Tr)}$ and $\boldsymbol{H}$ of dimension 3 × 2, 3 × 2 and 3 × 3, respectively, and both the vectors $\boldsymbol{F}$ and $\boldsymbol{G}$ with 3 elements.

For each constitutive model, initially the implementation of the model has been compared with reference results in the literature, in order to demonstrate the correctness of the results. Secondly, two 3D numerical examples have been solved, namely the compression of a cylinder under a uniform load and the compression due to a strip foundation. The numerical results are obtained by implementing the algorithm into the 3D FEM research code GeoMatFEM.

5.2. Numerical results validation

This section presents the validation of the results of the implemented framework.

For the Drucker-Prager model, the results of our implementation has been compared with those presented in de Souza Neto et al. (2009) for a 2D strip-footing collapse. Note that, the Drucker-Prager yield surface parameters are $\phi = 20$ and $coh = 0.49MPa$ (following the de Souza Neto et al. (2009) notation), which corresponds to $c = 1.0394MPa$ and $m = -0.7721$, assuming the outer cone approximation. The Fig. 3 shows the mesh of the benchmark and Fig. 4 presents the comparison between the reference results and the GeoMatFem computed results presented in this work. As can be observed, the results are almost identical. The very small differences are due to a different mesh discretization adopted in the reference example, a different convergence criteria and tolerance.

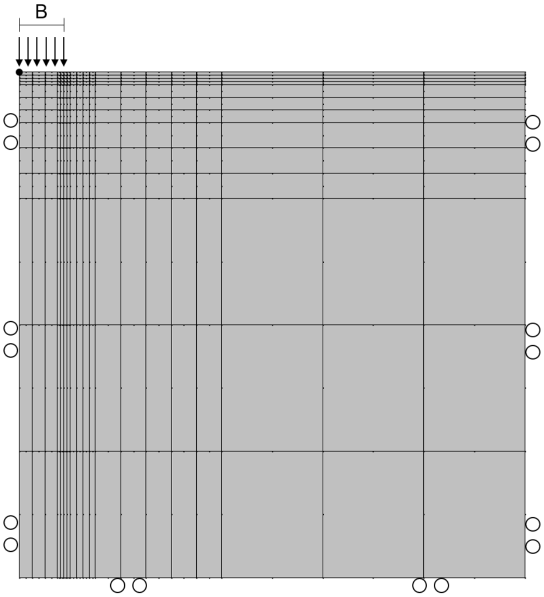

Figure 3: Mesh of the 2D benchmark for Drucker-Prager validation.

For the Modified Cam-Clay model, the results of our implementation has been compared with those presented in Borja et al. (1998) for a 2D flexible strip foundation. The benchmark is described in detail in the Section 4.2 in Borja

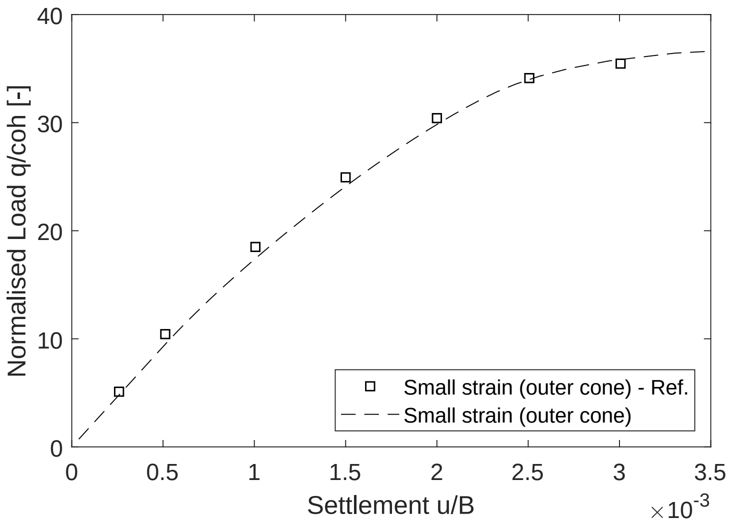

Figure 4: Comparison of the load-displacement curve with reference results for the Drucker-Prager model.

et al. (1998), and in particular the results are reported in the Figure 15 of the aforementioned reference. The Fig. 5 shows the mesh of the benchmark and Fig. 6 presents the comparison between the reference results and the GeoMat-Fem computed results presented in this work. As can be observed, the results are almost identical. The very small differences are due to a different mesh discretization adopted in the example and probably to a slightly different self weight initialization of the two simulations, which is not completely described in the reference paper.

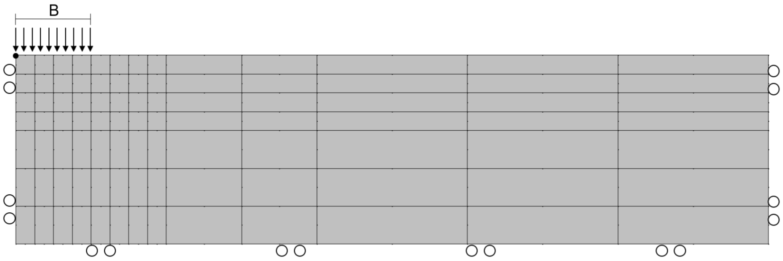

Figure 5: Mesh of the 2D benchmark for Modified Cam-Clay model validation.

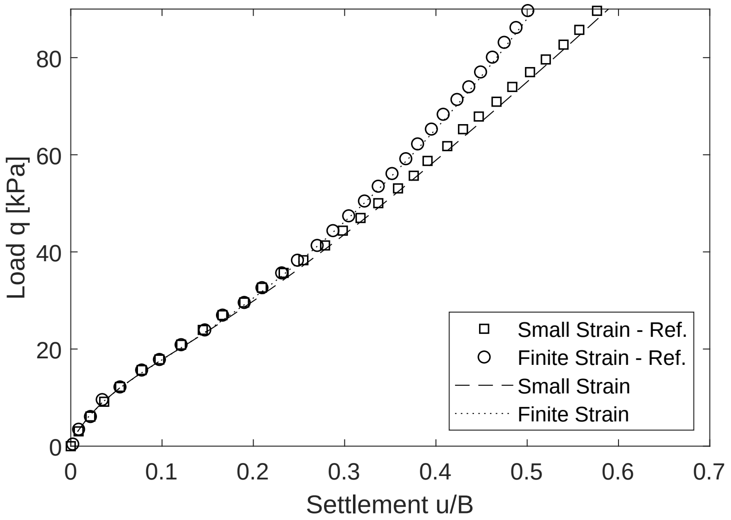

Figure 6: Comparison of the load-displacement curve with reference results for the Modified Cam-Clay model.

5.3. Test Case 1: compression of a cylinder

The first numerical test case deals with the uniform compression of a cylindrical specimen ($H = 100$ mm and $D = 50$ mm), discretized via 384 20-node hexahedral elements (Fig. 7). The base is fixed and the lateral surfaces are horizontally constrained; a vertical load is applied on the top surface by means of a uniform load equal to 0.20 MPa. The load is applied with 20 increments. The material data are reported in Table 8 and 9, for the Drucker-Prager and the Modified Cam-Clay model respectively, as presented in the previous section. The former is considered with ($h = 2.00$) and without ($h = 0.00$) hardening, the latter accounting for $\alpha = 0$, i.e. the volumetric and deviatoric deformations in the elastic regime are uncoupled (see Borja & Tamagnini (1998); Borja et al. (1997) for details). The relation between λ and k for small and finite strain has been computed according to Borja & Tamagnini (1998), i.e. $\hat{\lambda} = \tilde{\lambda}/(1 - \tilde{\lambda})$ and $\hat{k} = \tilde{k}/(1 - \tilde{k})$.

The resulting load-settlements curves for the top central node (denoted with the red color in Fig. 7) are depicted in Fig. 8. As it can be observed from Fig.

Parameter		
E	[MPa]	1.00
ν		0.30
m		0.50
c_0	[MPa]	0.01
$\bar{m}$		0.50
h		0.00 or 2.00

Table 8: Material parameters for the Drucker-Prager model in the cylindrical specimen.

Parameter	U.M.	Small strain	Finite strain
μ_0	MPa	2,0	2,0
α		0,0	0,0
$\tilde{k}$		0,0196	-
$\tilde{\lambda}$		0,1304	-
$\hat{k}$		-	0,02
$\hat{\lambda}$		-	0,15
M		1,00	1,00
p_0	MPa	-0,01	-0,01
p_{c0}	MPa	-0,01	-0,01
ϵ_{v0}^e		0,00	0,00

Table 9: Material parameters for the Modified Cam-Clay in the cylinder specimen.

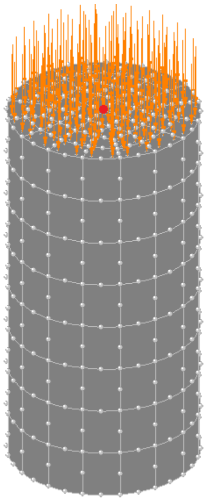

Figure 7: Discretized domain for a cylindrical specimen, with a uniform compression.

8, the final settlements with a finite strain approach are smaller if compared with a small strain analysis. When considering Finite Strain, the non-linear behavior is more evident, due to the concurrence of material and geometric non-linear effects. In order to better understand the mechanical soil behavior, let's consider also the stress paths in a P-Q plot together with the load-settlements curves presented in Fig. 8. As it can be observed in Fig. 9, the Drucker-Prager material presents initially (during the first four steps) a linear elastic behavior, and subsequently an elastoplastic one. In case of no hardening, the yield surface does not expand and the stress path is coincident with it, otherwise ($h = 2.00$) the yield surface shifts as far as the plastic deformation increases. If a Modified Cam-Clay model is accounted for, the response is elastoplastic from the beginning, and it is associated with an expansion of the elliptical yield surface.

More importantly, being the objective of the work to check the correctness of the procedure provided by a unifying scheme, Figs. 10 and 11 are to be considered, evidencing the convergence profiles of the global and local iterative schemes at some arbitrary time steps. In fact, the convergence profile is a litmus test in determining if the tangent operators are correctly implemented within

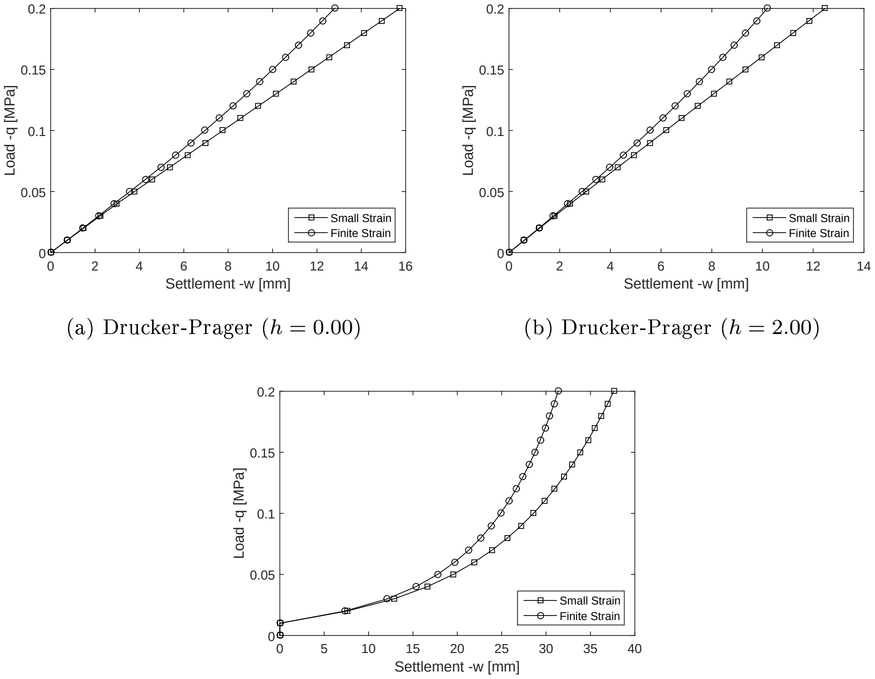

(a) Drucker-Prager ($h = 0.00$)

(b) Drucker-Prager ($h = 2.00$)

(c) Modified Cam-Clay

Figure 8: Vertical displacement of the top central node.

the FEM code. Both small and finite strain implementations are characterized by a fast convergence profile, asymptotically very close to the theoretical quadratic behavior. In case of the DP model, the local system of equations - required to solve the return mapping algorithm - is linear (even in the case of hardening, since the hardening law is linear), hence the solution is found in the first iteration (top plots in Fig. 11). Differently, if a MCC model is accounted for, even the local system of equations is highly non-linear, therefore also the local convergence profile exhibits the typical parabolic shape (bottom plots in Fig. 11).

5.4. Test Case 2: strip foundation

The second numerical test case considers the uniform compression of a strip foundation. The grid is sketched in Fig. 12, considering a typical domain of

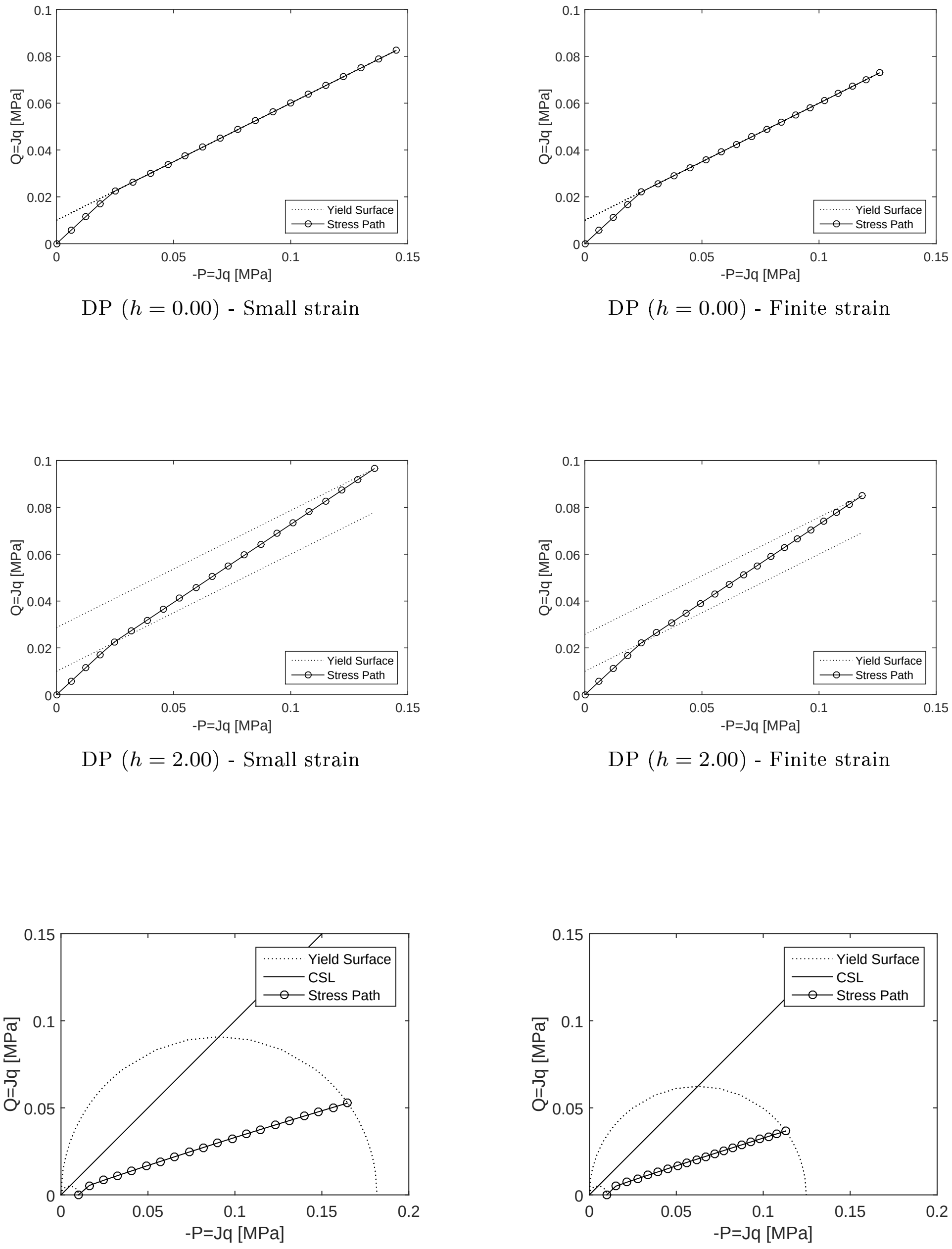

DP ($h = 0.00$) - Small strain

DP ($h = 0.00$) - Finite strain

DP ($h = 2.00$) - Small strain

DP ($h = 2.00$) - Finite strain

MCC - Small strain

MCC - Finite strain

Figure 9: Stress path in the P-Q diagram. The dotted line represents the yield surface.

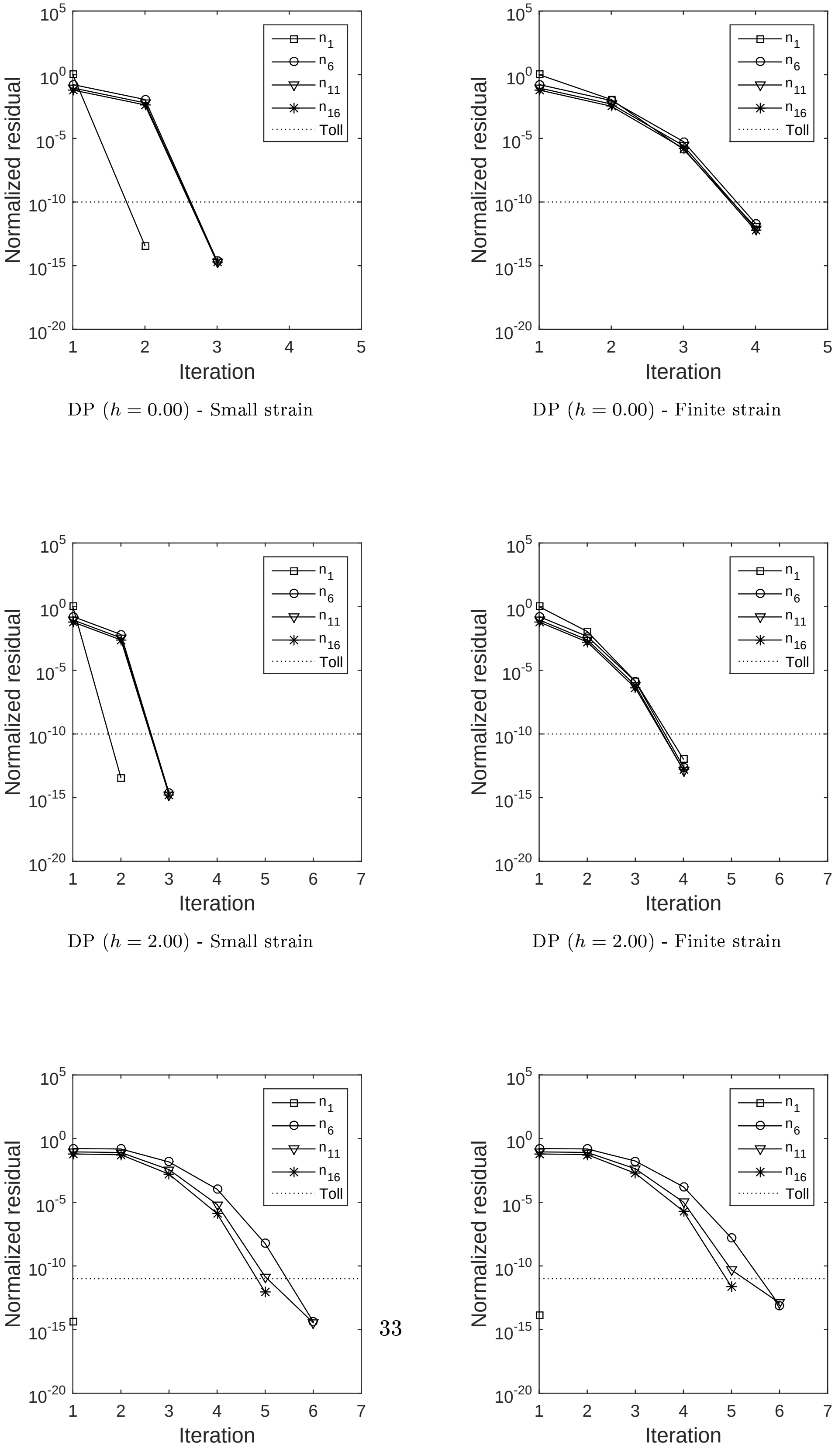

DP ($h = 0.00$) - Small strain

DP ($h = 0.00$) - Finite strain

DP ($h = 2.00$) - Small strain

DP ($h = 2.00$) - Finite strain

MCC - Small strain

MCC - Finite strain

Figure 10: Global convergence of Newton-Raphson iterations.

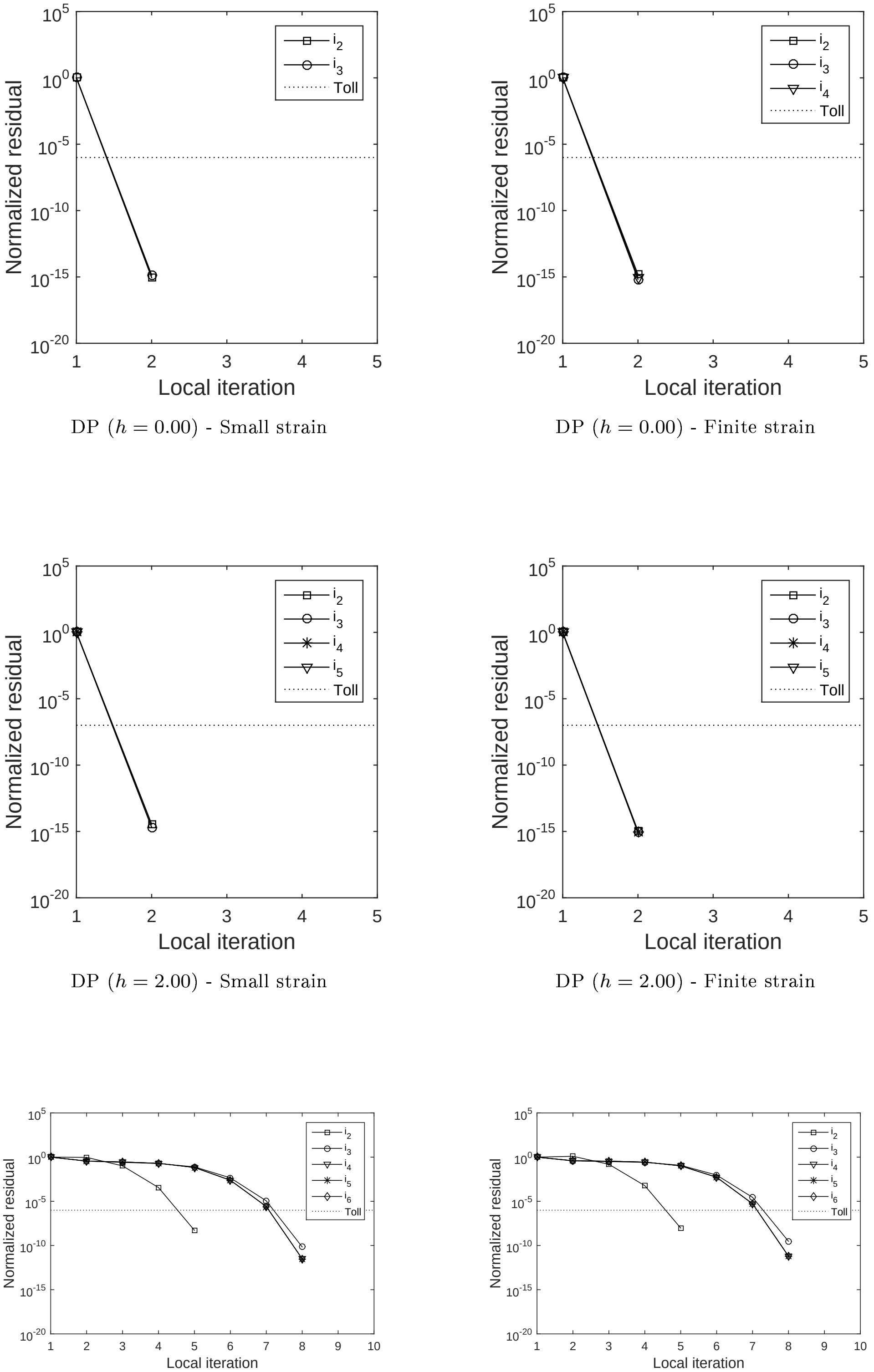

DP ($h = 0.00$) - Small strain

DP ($h = 0.00$) - Finite strain

DP ($h = 2.00$) - Small strain

DP ($h = 2.00$) - Finite strain

MCC - Small strain

MCC - Finite strain

Figure 11: Local convergence of Newton-Raphson iterations.

$30 \times 20\ m^2$, 1 m thick , discretized by 132 20-node hexahedral elements; the base is fixed and the lateral surfaces are constrained to reconstruct plane strain conditions. A uniform load of $0,10$ MPa is applied, by means of 30 equal increments, on top to the first 5 m length. The load-settlements curves of the top node along the left border (namely the red node A in Fig. 12) are depicted in Fig. 13. The material data are shown in Table 10 and 11, for the Drucker-Prager and the Modified Cam-Clay material, respectively.

Even if the material response is more evidently non-linear for both Drucker-Prager and Modified Cam-Clay models than the previous case, no appreciable differences arise from a linear or non-linear geometric approach.

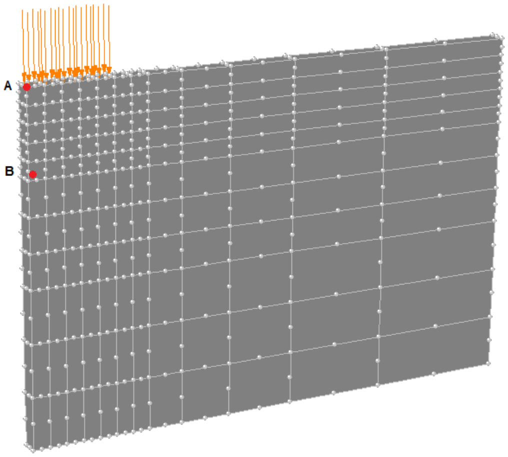

Figure 12: Discretized domain for strip a foundation.

Anyway, when considering efficiency and robustness of the numerical scheme for the implementation of the elastoplastic laws, Figs. 14 and 15 show again convergence profiles exhibiting a shape very close to the theoretical quadratic one, therefore newly confirming the correct implementation of both the local and global tangent operators and the strength of the developed algorithm. Particularly, looking at Fig. 15 for the DP material it can be observed that the solution is achieved via one iteration, since the system to be solved is linear. On the other hand, for the MCC model the set of local equations is non-linear and

Parameter		
E	[MPa]	1.00
ν		0.30
m		0.50
c	[MPa]	0.02
$\bar{m}$		0.50
h		0

Table 10: Material parameters for the Drucker-Prager model in the strip foundation.

Parameter	U.M.	Small strain	Finite strain
μ_0	MPa	2,0	2,0
α		0,0	0,0
$\tilde{k}$		0,0196	-
$\tilde{\lambda}$		0,1304	-
$\hat{k}$		-	0,02
$\hat{\lambda}$		-	0,15
M		1,00	1,00
p_0	MPa	-0,05	-0,05
p_{c0}	MPa	-0,05	-0,05
ϵ^e_{v0}		0,00	0,00

Table 11: Material parameters for the Modified Cam-Clay in the strip foundation.

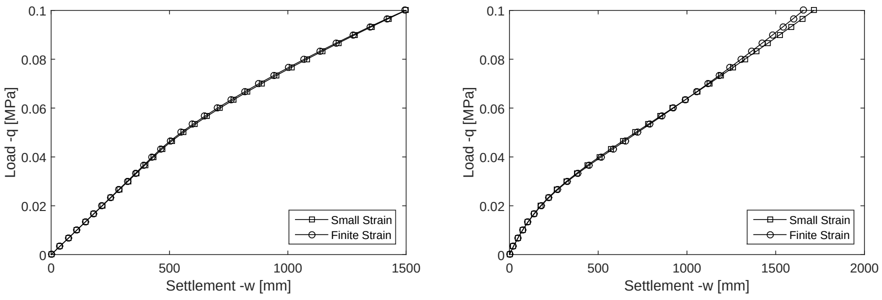

(a) Drucker-Prager

(b) Modified Cam-Clay

Figure 13: Vertical displacement of the selected node due to the increase of the vertical uniform load.

therefore the convergence profile exhibits a shape very close to the theoretical quadratic one (as already previously evidenced). If we observe the global convergence profile in Fig. 14, the quadratic convergence for MCC is confirmed, whereas for DP the shape is first bilinear (elastic response), then quadratic.

As a conclusion remark, we computed the performance in terms of computational cost of the proposed framework with respect to the traditional one. Indeed, we considered the computational cost at the element level, i.e. the time required to compute the stress update and the consistent tangent operator in a single element, for all the Gauss Point. In order to have a more significant value and a more useful comparison, we considered a single iteration in the global N-R loop, and we averaged the element computational time for all the element where at least one Gauss Point experienced an elastoplastic behaviour. The performance has been computed using a Matlab code on a laptop with Intel i7-8565U CPU at 1.80GHz processors. The speed up is described in the Table 12. As can be observed, there is a slightly speed up in the computational cost, but in general the computational time is in line with the traditional way. This is not surprising since, the two formulations solve almost the same number of equations, and with a similar complexity. In the implementation of elastoplastic models, usually what kills the computational performances is related to a wrong

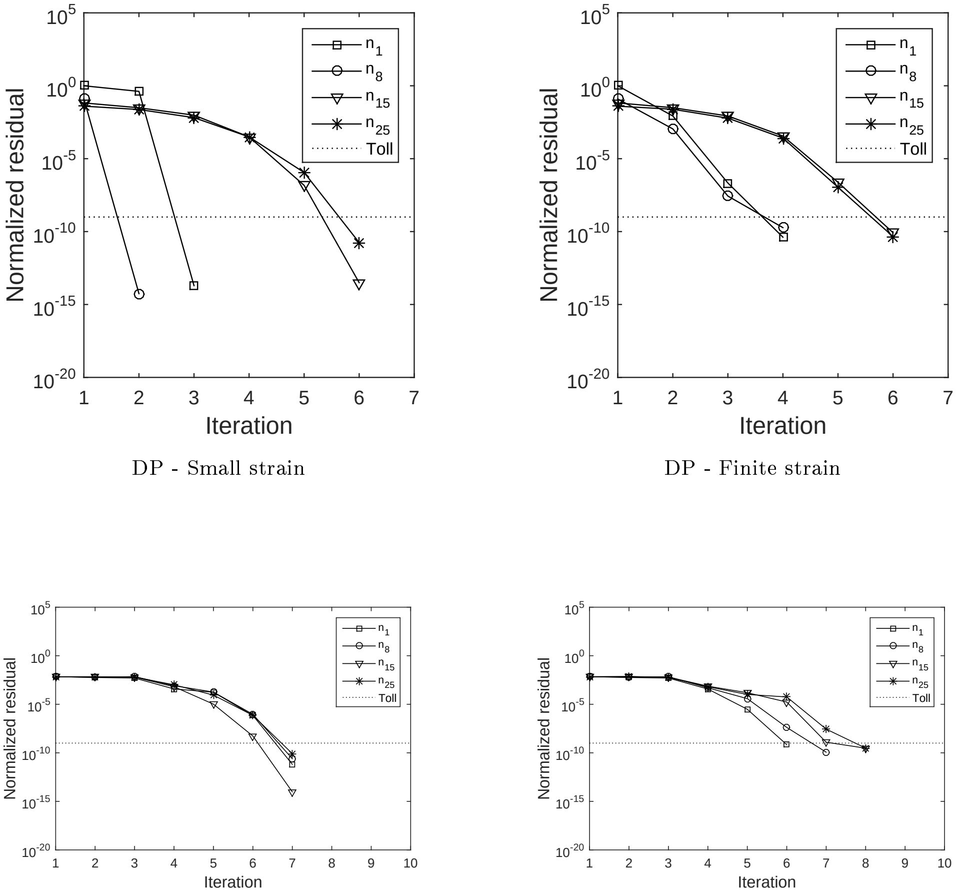

DP - Small strain

DP - Finite strain

MCC - Small strain

MCC - Finite strain

Figure 14: Global convergence of N–R iterations.

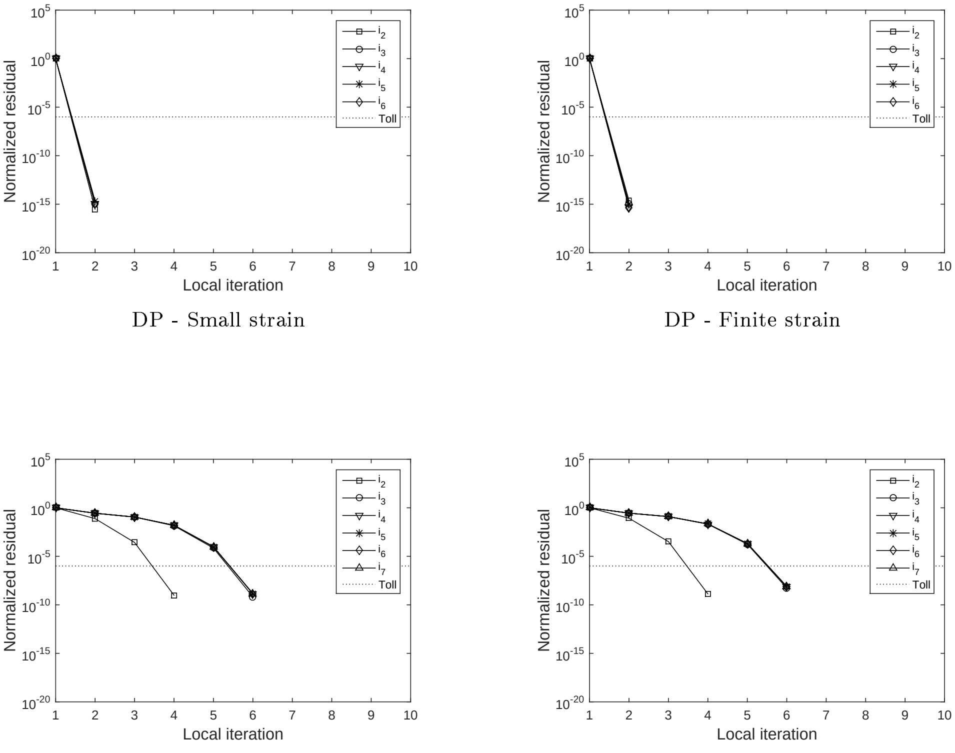

DP - Small strain

DP - Finite strain

MCC - Small strain

MCC - Finite strain

Figure 15: Local convergence of Newton-Raphson iterations.

Model	Ave. Computational Time [s]		Speed-up [%]
	Traditional	New Gen. Framework	
Drucker-Prager	0,0277	0,0263	-5,05
Modified Cam-Clay	0,0325	0,0302	-7,08

Table 12: Comparison of the Computational Time of the general framework with respect to the traditional implementation.

computation of the tangent operator in the N-R scheme, both at a local and a global level. As demonstrated by the examples, this framework helps in the correct computation of both the tangent operators.

6. Conclusions

A unified framework has been here presented and described, specifically designed to develop and implement elastoplastic constitutive laws defined in the so called two-invariants space, both in small and finite strain. A schematic procedure has been proposed to directly compute the two algorithmic tangent operators, necessary to solve the NR scheme at the local and global level. Even if implemented within a FE code referring to two typical elastoplastic models (i.e. Drucker-Prager and Modified Cam-Clay), the procedure is fully general and can be applied to any elastoplastic formulation described in the space of the two-invariants. Two numerical test cases have allowed for proving the correctness of the implementation as well as the strength of the proposed algorithm.

References

Aravas, N. (1987). On the numerical integration of a class of pressure-dependent plasticity models. *International Journal for numerical methods in engineering*, *24*, 1395–1416.

Aubertin, M., & Li, L. (2004). A porosity-dependent inelastic criterion for engineering materials. *International Journal of Plasticity*, *20*, 2179–2208. URL: http://www.sciencedirect.com/science/article/pii/S0749641904000634. doi:10.1016/j.ijplas.2004.05.004.

Bao, J. Q., Long, X., Tan, K. H., & Lee, C. K. (2013). A new generalized Drucker-Prager flow rule for concrete under compression. *Engineering Structures*, *56*, 2076–2082. doi:10.1016/j.engstruct.2013.08.025.

Borja, R. I. (2013). *Plasticity. Modeling and Computation*. Springer.

Borja, R. I., Kossi, M. S., & Pablo, F. S. (2003). On the numerical integration of three-invariant elastoplastic constitutive models. *Comput. Methods. Appl. Mech. Engrg.*, *192*, 1227–1258.

Borja, R. I., & Tamagnini, C. (1998). Cam-Clay plasticity Part III: Extension of the infinitesimal model to include finite strains. *Comput. Methods. Appl. Mech. Engrg.*, *155*, 73–95.

Borja, R. I., Tamagnini, C., & Alarcón, E. (1998). Elastoplastic consolidation at finite strain part 2: finite element implementation and numerical examples. *Computer Methods in Applied Mechanics and Engineering*, *159*, 103–122.

Borja, R. I., Tamagnini, C., & Amorosi, A. (1997). Coupling plasticity and energy-conserving elasticity models for clays. *Journal of geotechnical and geoenvironmental engineering*, *123*, 948–957.

Carvalho, R. P., Lopes, I. A. R., & Pires, F. M. A. (2018). Prediction of the yielding behaviour of ductile porous materials through computational homogenization. *Engineering Computations*, .

Cecilio, D. L., Devloo, P. R., Gomes, S. M., dos Santos, E. R., & Shauer, N. (2015). An improved numerical integration algorithm for elastoplastic constitutive equations. *Computers and Geotechnics*, *64*, 1–9.

Čermák, M., Sysala, S., & Valdman, J. (2019). Efficient and flexible matlab implementation of 2d and 3d elastoplastic problems. *Applied Mathematics and Computation*, *355*, 595–614.

Coelho, M., & Roehl, D. (2019). A finite–strain elastoplasticity material model for etfe membrane structures. *Computers and Structures*, *217*, 36–44. URL: `https://www.sciencedirect.com/science/article/pii/S0045794917311860`. doi:`https://doi.org/10.1016/j.compstruc.2019.03.007`.

Drucker, D. C., & Prager, W. (1952). Soil mechanics and plastic analysis or limit design. *Quarterly of applied mathematics*, *10*, 157–165.

Govindarajan, R., & Aravas, N. (1995). Pressure-dependent plasticity models: Loading–unloading criteria and the consistent linearization of an integration algorithm. *Communications in numerical methods in engineering*, *11*, 339–345.

Gudimetla, M. R., & Doghri, I. (2017). A finite strain thermodynamically-based constitutive framework coupling viscoelasticity and viscoplasticity with application to glassy polymers. *International Journal of Plasticity*, *98*, 197 – 216. URL: `http://www.sciencedirect.com/science/article/pii/S0749641917301286`. doi:`https://doi.org/10.1016/j.ijplas.2017.08.001`.

Halilovic, M., Starman, B., Vrh, M., & Stok, B. (2017). A robust explicit integration of elasto-plastic constitutive models, based on simple subincrement size estimation. *Engineering Computations*, .

Hu, Q., Li, X., Han, X., Li, H., & Chen, J. (2017). A normalized stress invariant-based yield criterion: Modeling and validation. *International Journal of Plasticity*, *99*, 248 – 273. URL: `http://www.sciencedirect.com/science/article/pii/S0749641917301043`. doi:`https://doi.org/10.1016/j.ijplas.2017.09.010`.

Indriyantho, B. R., Zreid, I., & Kaliske, M. (2020). A nonlocal softening plasticity based on microplane theory for concrete at finite strains. *Computers and Structures*, *241*, 106333. URL: `https:`

//www.sciencedirect.com/science/article/pii/S004579492030136X. doi:https://doi.org/10.1016/j.compstruc.2020.106333.

Isbuga, V., & Regueiro, R. A. (2017). Finite element analysis of finite strain micromorphic drucker-prager plasticity. *Computers & Structures*, *193*, 31–43.

Khan, A. S., & Huang, S. (1995). *Continuum theory of plasticity*. John Wiley & Sons.

Lai, Y., Liao, M., & Hu, K. (2016). A constitutive model of frozen saline sandy soil based on energy dissipation theory. *International Journal of Plasticity*, *78*, 84–113. URL: http://linkinghub.elsevier.com/retrieve/pii/S0749641915001837. doi:10.1016/j.ijplas.2015.10.008.

Lee, E. H. (1969). Elastic-plastic deformations at finite strains. *Journal of Applied Mechanics*, *36*, 1–6.

Lee, K., Marimuthu, K. P., Han, J., & Lee, H. (2021). Enhancement of drucker-prager yield model by adding corner points for pressure-dependent materials. *Journal of Mechanical Science and Technology*, *35*, 1017–1027.

Lloret-Cabot, M., Pineda, J. A., & Sheng, D. (2018). Numerical implementation of a critical state model for soft rocks. In *PanAm Unsaturated Soils 2017* (pp. 236–246).

Mohammadi, M., Dai, J.-G., Wu, Y.-F., & Bai, Y.-L. (2019). Development of extended drucker–prager model for non-uniform frp-confined concrete based on triaxial tests. *Construction and Building Materials*, *224*, 1–18.

De la Morena, G., Asensio, L., Navarro, V., & Yustres, Á. (2017). A simple procedure to improve the explicit integration of cam-clay models. *Computers and Geotechnics*, *81*, 207–211.

Mourad, H., Bronkhorst, C., Livescu, V., Plohr, J., & Cerreta, E. (2017). Modeling and simulation framework for dynamic strain localization in elasto-viscoplastic metallic materials subject to large deformations. *International Journal of Plasticity*, *88*, 1 – 26. URL: http://www.sciencedirect.com/science/article/pii/S0749641916301668. doi:https://doi.org/10.1016/j.ijplas.2016.09.009.

Neuner, M., Gamnitzer, P., & Hofstetter, G. (2020). A 3d gradient-enhanced micropolar damage-plasticity approach for modeling quasi-brittle failure of cohesive-frictional materials. *Computers and Structures*, *239*, 106332. URL: https://www.sciencedirect.com/science/article/pii/S0045794920301358. doi:https://doi.org/10.1016/j.compstruc.2020.106332.

Ogden, R. W. (1997). *Non-linear elastic deformations*. Courier Corporation.

Peng, Q., & Chen, M. (2012). An efficient return mapping algorithm for general isotropic elastoplasticity in principal space. *Computers & Structures*, *92*, 173–184.

Rawat, A., Piska, R., Rajagopal, A., & Hossain, M. (2021). Nonlocal plasticity-based damage modeling in quasi-brittle materials using an isogeometric approach. *Engineering Computations*, .

Roscoe, K., & Burland, J. (1968). On the generalized stress-strain behaviour of wet clay, .

Sanei, M., Duran, O., Devloo, P. R., & Santos, E. S. (2020). An innovative procedure to improve integration algorithm for modified cam-clay plasticity model. *Computers and Geotechnics*, *124*, 103604.

Simo, J. (1992). Algorithms for static and dynamic multiplicative plasticity that preserve the classical return mapping schemes of the infinitesimal theory. *Computer Methods in Applied Mechanics and Engineering*, *99*, 61–112.

Simo, J. C., & Hughes, T. J. (2006). *Computational inelasticity* volume 7. Springer Science & Business Media.

de Souza Neto, E. A., Peric, D., & Owen, D. R. J. (2009). *Computational Methods for Plasticity: Theory and Applications*. John Wiley and Sons.

Späth, M., Herrmann, C., Prajapati, N., Schneider, D., Schwab, F., Selzer, M., & Nestler, B. (2021). Multiphase-field modelling of crack propagation in geological materials and porous media with drucker-prager plasticity. *Computational Geosciences*, *25*, 325–343.

Spiezia, N., Salomoni, V. A., & Majorana, C. E. (2016). Plasticity and strain localization around a horizontal wellbore drilled through a porous rock formation. *International Journal of Plasticity*, *78*, 114–144.

Tavoosi, M., Sharifian, M., & Sharifian, M. (2019). A hybrid method to update stress for perfect von-mises plasticity coupled with lemaitre damage mechanics. *Engineering Computations*, .

Wei, S.-M., Yuan, L., & Cui, Z.-D. (2021). Application of closest point projection method to unified hardening model. *Computers and Geotechnics*, *133*, 104064.

Weng, M.-C., & Ling, H. I. (2013). Modeling the behavior of sandstone based on generalized plasticity concept. *International Journal for Numerical and Analytical Methods in Geomechanics*, *37*, 2154–2169.

Yilmaz, M. (2019). Easy pre/post-processing of finite elements with custom symbolic-objects: A self-expressive python interface. *Computers and Structures*, *222*, 82–97. URL: `https://www.sciencedirect.com/science/article/pii/S0045794918316341`. doi:`https://doi.org/10.1016/j.compstruc.2019.07.002`.

Zhao, G.-F., Lian, J., Russell, A., & Khalili, N. (2019). Implementation of a modified drucker–prager model in the lattice spring model for plasticity and fracture. *Computers and Geotechnics*, *107*, 97–109.